Editors' Suggestion

Global topological synchronization of weighted simplicial complexes

Runyue Wang,[1,*] Riccardo Muolo,[2] Timoteo Carletti,[3] and Ginestra Bianconi[1,4,†]

[1]*School of Mathematical Sciences, Queen Mary University of London, London E1 4NS, United Kingdom*

[2]*Department of Systems and Control Engineering, Tokyo Institute of Technology, 2 Chome-12-1 Ookayama, Meguro-ku, Tokyo 152-8552, Japan*

[3]*Department of Mathematics and naXys, Namur Institute for Complex Systems, University of Namur, Rue Grafé 2, B5000 Namur, Belgium*

[4]*The Alan Turing Institute, The British Library, London NW1 2DB, United Kingdom*

(Received 17 April 2024; accepted 17 June 2024; published 31 July 2024)

Higher-order networks are able to capture the many-body interactions present in complex systems and to unveil fundamental phenomena revealing the rich interplay between topology, geometry, and dynamics. Simplicial complexes are higher-order networks that encode higher-order topology and dynamics of complex systems. Specifically, simplicial complexes can sustain topological signals, i.e., dynamical variables not only defined on nodes of the network but also on their edges, triangles, and so on. Topological signals can undergo collective phenomena such as synchronization, however, only some higher-order network topologies can sustain global synchronization of topological signals. Here we consider global topological synchronization of topological signals on weighted simplicial complexes. We demonstrate that topological signals can globally synchronize on weighted simplicial complexes, even if they are odd-dimensional, e.g., edge signals, thus overcoming a limitation of the unweighted case. These results thus demonstrate that weighted simplicial complexes are more advantageous for observing these collective phenomena than their unweighted counterpart. In particular, we present two weighted simplicial complexes: the weighted triangulated torus and the weighted waffle. We completely characterize their higher-order spectral properties and demonstrate that, under suitable conditions on their weights, they can sustain global synchronization of edge signals. Our results are interpreted geometrically by showing, among the other results, that in some cases edge weights can be associated with the lengths of the sides of curved simplices.

DOI: 10.1103/PhysRevE.110.014307

I. INTRODUCTION

Higher-order networks [1–4] encode for the many-body interactions of complex systems ranging from brain [5,6] to collaboration networks [7,8] and are transforming our understanding of the relation existing between network topology, geometry, and dynamics [2,9–12]. Until now, in the majority of the works available in the literature, the description of the dynamical state of a network has been dominated by the node-centered point of view in which dynamical variables are only associated to the nodes of the network. This approach has also provided relevant results in the context of higher-order networks on papers involving epidemics and opinion dynamics [13–15], game theory [16], random walks [17], pattern formation [18], percolation [19–24], synchronization [25–34]. While this approach is certainly relevant in some contexts, for instance, in epidemic spreading where we consider the state of the nodes and individuals as susceptible, infected, and recovered, in general, restricting the focus only to nodes dynamical states is a limitation. Recently, great attention [9,35–49] has been addressed to topological signals, i.e., dynamical variables associated not only to nodes but also to edges, triangles, and higher-dimensional simplices of simplicial complexes. Edge signals are ubiquitous and include biological transportation networks [50–52], synaptic signals, and edge signals at the level of brain regions [53,54]. Further examples of edge signals are currents in the ocean [39,55] and speed of wind which are vector fields that can be projected onto edges of a tessellation of the surface of the Earth. Examples of topological signals associated with higher-dimensional simplices are, for instance, citations gathered by a team of collaborators.

Topological signals can undergo collective phenomena such as synchronization transitions captured by the topological Kuramoto model [35,36] and its variations on directed and weighted simplicial complexes [41,56], and also Dirac synchronization [40,48,57] by coupling topological signals of different dimensions to each other. These models reveal that topology shapes dynamics and that the synchronized state is localized along the harmonic eigenvectors of the simplicial complex, the latter being localized around higher-dimensional holes of the simplicial complex and, thus, in general, are not uniform on the simplices of the higher-order network.

*Contact author: runyue.wang@qmul.ac.uk
†Contact author: ginestra.bianconi@gmail.com

Having established that higher-order topological signals can synchronize as described by the topological Kuramoto model, an important question is whether global topological synchronization (GTS) can be ever observed, the latter referring to a state of higher-order topological signals in which each simplex undergoes the same dynamics. For instance, the GTS of the edge signal implies that every edge of the simplicial complex exhibits the same dynamics; similarly GTS of triangle signals implies that the dynamical variable associated to every triangle of the simplicial complex evolves in unison, and so on.

In Ref. [37], the conditions for observing GTS of topological signals have been derived for unweighted simplicial and cell complexes. There it has been found that topological signals can undergo GTS only for specific higher-order network topologies. This is in contrast to what happens in a connected network where node signals always admit a global synchronized state and the only remaining problem is whether this state is dynamically stable, leading to the famous master stability function (MSF) approach [58,59]. Specific unweighted higher-order network topologies on which topological signals can globally synchronize are square and cubic lattices with periodic boundary conditions forming, respectively a two-dimensional and three-dimensional cell complex tessellating a two-dimensional and three-dimensional torus [37]. Other examples of topologies in which GTS of $(d-1)$-topological signals can always occur are d-dimensional discrete manifolds. However, in Ref. [37] it has been also found that, as long as the simplicial complexes are unweighted, odd topological signals can never synchronize.

In this paper, we take one step further in the understanding of GTS by investigating the conditions for the emergence of GTS on weighted simplicial complexes. We found that under suitable conditions on the simplices weights, odd-dimensional signals can also synchronize on some simplicial complexes. Specifically, we analyze in detail the GTS of edge signals on weighted simplicial complexes, this being a setting where GTS can never emerge in the unweighted case. We provide two examples of weighted simplicial complexes, the weighted triangulated torus (WTT) and the weighted waffle (WW), and by performing a comprehensive study of their higher-order spectral properties, we prove that they can sustain global synchronization of edge signals when their edge weights satisfy suitable conditions.

Our results demonstrate that varying edge weights of a given simplicial complex can allow for a transition from a state capable of sustaining GTS to a state in which the latter is forbidden. The possibility of achieving or obstructing synchronization by tuning the weights of the simplices is of potential interest to the control community, where tools from network science and complex systems are becoming increasingly popular [60]. In fact, the control of synchronization is of paramount importance in many natural and engineered systems, such as the brain [61,62] or power grids [63], relevant results in this direction are already known for pairwise networks [64,65], and this framework has recently been extended to systems with higher-order interactions [66]. Given the higher-order nature of interactions in the brain [5,6], the possibility of using the weights of the simplices as a control parameter can be particularly interesting, for instance, in the design of efficient methods to prevent the synchronization of certain brain regions during seizures [67].

In this paper, we also analyze the relation existing among the conditions on the weights required to allow for GTS and the underlying geometry of the simplicial complexes. Specifically, we address the important theoretical question of whether the conditions that guarantee GTS can admit a geometrical interpretation. We found that the WTT can admit a geometrical interpretation where all the edge capacitances are the same and the simplices are curved. Furthermore, we provide a comprehensive mathematical framework by exploring more general geometrical interpretations of the weights of the edges.

This paper is structured as follows. In Sec. II, we introduce the basic notions about (weighted) simplicial complexes needed to describe topological dynamical systems in the following Sec. III. The developed theory will be presented by using two weighted simplicial complexes defined and characterized in Sec. IV. The dynamical behaviors resulting from the use of those higher-order structures will be discussed in Sec. V while their geometrical properties will be analyzed in Sec. VI. Eventually, in Sec. VII, we summarize our results.

II. FUNDAMENTAL PROPERTIES OF WEIGHTED SIMPLICIAL COMPLEXES

A. Weighted simplicial complexes

A simplex of dimension n is a set of $n+1$ nodes, thus a 0-simplex is a node, a 1-simplex is an edge, a 2-simplex is a triangle, and so on. The faces of an n-dimensional simplex α are the n'-dimensional simplices α' $(n' < n)$ formed by a proper subset of the nodes of α. A simplicial complex $\mathcal{K}$ is a set of simplices closed under the inclusion of the faces. The dimension d of a simplicial complex is the largest dimension of its simplices.

We consider a generic weighted d-dimensional simplicial complex formed by N_n simplices of dimension n, i.e., N_0 nodes, N_1 edges, N_2 triangles, and so on. The simplices have an orientation induced by the node labels. Each simplex α is assigned a weight $w_\alpha > 0$. We adopt the following notation: If a n-dimensional simplex α is oriented coherently with one of its $(n-1)$-dimensional face α' we write $\alpha \sim \alpha'$. Conversely, if the simplex α is incoherently oriented with its face α', we write $\alpha \not\sim \alpha'$.

B. Topological signals

The n-dimensional topological signal comprises the set of dynamical variables associated to each n-dimensional simplex of the simplicial complex. The n-dimensional topological signal $\boldsymbol{\phi}$ is mathematically defined as n-cochain, i.e., $\boldsymbol{\phi} \in C^n$, and can be represented as a N_n column vector of elements ϕ_α associated to the n-dimensional simplex α with the additional property that if $\alpha \to -\alpha$, i.e., if the orientation of the simplex α is flipped, then $\phi_\alpha \to -\phi_\alpha$. To have an intuition of this property, consider the current defined on the edge $[i, j]$ and going from node i to node j, this current will be considered to be positive if the edge is oriented from node i to node j, while it will be negative if the opposite orientation is adopted.

The notion of a topological signal allows us to completely describe the dynamics of a simplicial complex going beyond

the node-centered approach that associates a dynamical state only to their nodes. Among topological signals, edge signals are particularly interesting and present in a large variety of real systems. The latter can describe fluxes and currents associated with biological transportation networks [50–52]. Additionally, edge signals can be used to capture and process the speed of winds and currents of the ocean in climate research [39,47,55]. Recently, edge signals have raised increasing attention in brain research [53,54] as they do not only capture synaptic signals at the neuronal level but also edge signals at the level of brain regions.

C. Weighted Hodge Laplacians

The topology of the simplicial complex is encoded by the $N_{n-1} \times N_n$ boundary matrices $\mathbf{B}_{[n]}$ of elements

$$[\mathbf{B}_{[n]}]_{\alpha',\alpha} = \begin{cases} 1 & \text{if} \quad \alpha \sim \alpha' \\ -1 & \text{if} \quad \alpha \not\sim \alpha' \\ 0 & \text{otherwise.} \end{cases}$$

The boundary matrix $\mathbf{B}_{[n]}$ maps the N_n simplices of the simplicial complex to the N_{n-1} simplices at its boundary. The boundary matrices $\mathbf{B}_{[n]}$ fully characterize the topology of the simplicial complex and are pivotal in defining the weighted Hodge Laplacians that determine the higher-order diffusion properties on the weighted simplicial complex.

The weighted Hodge Laplacian will be defined in terms of the weighted boundary matrices, which take into account the metric associated to the simplicial complex. Specifically, on a weighted simplicial complex, we define the weighted boundary matrix $\mathcal{B}_{[n]}$ given by

$$\mathcal{B}_{[n]} = \mathbf{G}_{[n-1]}^{1/2} \mathbf{B}_{[n]} \mathbf{G}_{[n]}^{-1/2}, \tag{1}$$

expressed in terms of the $N_n \times N_n$ diagonal metric matrices $\mathbf{G}_{[n]}$ whose diagonal elements are given by the inverse of the weights w_α, i.e.,

$$\mathbf{G}_{[n]}([\alpha,\alpha]) = \frac{1}{w_\alpha}. \tag{2}$$

The n-order symmetric weighted Hodge Laplacian $\mathbf{L}_{[n]}$ [68,69] is a $N_n \times N_n$ matrix that describes the diffusion from n-simplices to n-simplices either through $(n-1)$ or through $(n+1)$-dimensional simplices. It is defined as

$$\mathbf{L}_{[n]} = \mathbf{L}_{[n]}^{\text{up}} + \mathbf{L}_{[n]}^{\text{down}}, \tag{3}$$

with

$$\begin{aligned} \mathbf{L}_{[n]}^{\text{up}} &= \mathcal{B}_{[n+1]} \mathcal{B}_{[n+1]}^{\top}, \\ \mathbf{L}_{[n]}^{\text{down}} &= \mathcal{B}_{[n]}^{\top} \mathcal{B}_{[n]}, \end{aligned} \tag{4}$$

where $\mathcal{B}_{[n]}$ is the weighted boundary matrix defined in Eq. (1). From the definition of $\mathbf{L}_{[n]}^{\text{up}}$ and $\mathbf{L}_{[n]}^{\text{down}}$, it is immediate to check that the nonzero spectrum of $\mathbf{L}_{[n]}^{\text{down}}$ coincides with the nonzero spectrum of $\mathbf{L}_{[n-1]}^{\text{up}}$. Additionally, we note that the symmetric Hodge Laplacian defined in Eqs. (3) and (4) obeys the Hodge decomposition. In fact, we have

$$\mathbf{L}_{[n]}^{\text{up}} \mathbf{L}_{[n]}^{\text{down}} = \mathbf{0}, \quad \mathbf{L}_{[n]}^{\text{down}} \mathbf{L}_{[n]}^{\text{up}} = \mathbf{0}. \tag{5}$$

This implies that every signal defined on n-dimensional simplices, (i.e., every n-cochain $\boldsymbol{\phi} \in C^n$) can be decomposed in a unique way as

$$\boldsymbol{\phi} = \boldsymbol{\phi}^{\text{harm}} + \mathcal{B}_{[n+1]} \boldsymbol{\phi}^{[+]} + \mathcal{B}_{[n]}^{\top} \boldsymbol{\phi}^{[-]}, \tag{6}$$

where $\boldsymbol{\phi}^{[+]} \in C^{n+1}$ and $\boldsymbol{\phi}^{[-]} \in C^{n-1}$. Another important consequence of Hodge decomposition is that any nonzero eigenvalue $\Lambda_{[n]}$ of the nth Hodge Laplacian $\mathbf{L}_{[n]}$ is either a nonzero eigenvalue of $\mathbf{L}_{[n]}^{\text{down}}$ or a nonzero eigenvalue of $\mathbf{L}_{[n]}^{\text{up}}$.

III. TOPOLOGICAL GLOBAL SYNCHRONIZATION

Can topological signals globally synchronize? This important research question requires us to consider the dynamics of identical topological oscillators. Given the nth order topological signal $\boldsymbol{\phi}$ with elements $\phi_\alpha \in \mathbb{R}^m$, the GTS obeys the dynamics

$$\frac{d\boldsymbol{\phi}_\alpha}{dt} = F(\boldsymbol{\phi}_\alpha) - \sigma \sum_{\alpha' \in Q_n} [\mathbf{L}_{[n]}]_{\alpha,\alpha'} h(\boldsymbol{\phi}_{\alpha'}), \tag{7}$$

where the functions F and h are taken elementwise with $F(\phi_\alpha) \in \mathbb{R}^m$ and $h(\phi_\alpha) \in \mathbb{R}^m$, $\mathbf{L}_{[n]}$ indicates the Hodge Laplacian, and σ is the coupling constant. Here Q_n indicates the set of all the n-dimensional simplices of the simplicial complex $\mathcal{K}$. To guarantee the equivariance of this dynamical equation under changes of orientation of the simplices, we need F and h to be odd functions, although these functions do not have other limitations.

If we consider exclusively node signals ($n = 0$), a globally synchronized dynamical state of Eq. (7) exists for any arbitrary connected network. A global synchronized state refers to the state in which each oscillator follows the same dynamics, i.e., $\boldsymbol{\phi}_\alpha = \boldsymbol{\omega}(t)$ with $\dot{\boldsymbol{\omega}} = \mathbf{F}(\boldsymbol{\omega})$. This implies that the topological signal is given by $\boldsymbol{\phi} = \boldsymbol{\omega}(t) \otimes \mathbf{1}_{N_n}$. Since on a connected network the constant eigenvector $\mathbf{1}_{N_0}$ is the unique harmonic eigenvector of the graph Laplacian $\mathbf{L}_{[0]}$, the global synchronized state of node signal exists for any (connected) network. The key question that needs to be answered is thus whether this dynamical state is stable. The MSF framework [58,59] is a powerful framework to assess whether the global synchronization state is stable. However, for higher-order topological signals with $n > 0$, the constant eigenvector $\mathbf{1}_{N_n}$ is not guaranteed to be in the kernel of $\mathbf{L}_{[n]}$, hence $\boldsymbol{\phi} = \boldsymbol{\omega}(t) \otimes \mathbf{1}_{N_n}$ is not a solution of the GTS.

Note that an additional complexity of the problem arises from the fact that for topological signals, the synchronized state is a cochain, i.e., it has a sign depending on the orientation of the simplices. This implies that, strictly speaking, a global synchronized state is proportional to the eigenvector $\mathbf{u}$ with elements $|u_i| = 1$.

It follows that only simplicial or cell complexes admitting $\mathbf{u}$ in the kernel of the Hodge Laplacian $\mathbf{L}_{[n]}$ can display global synchronization. Specifically, to observe global synchronization we must impose

$$\mathbf{L}_{[n]} \mathbf{u} = \mathbf{0}, \tag{8}$$

which due to Hodge decomposition implies

$$\mathbf{L}_{[n]}^{\text{up}} \mathbf{u} = \mathbf{0}, \quad \mathbf{L}_{[n]}^{\text{down}} \mathbf{u} = \mathbf{0}. \tag{9}$$

On topologies for which the global synchronized state exists, it is necessary to also check whether this dynamical state

is stable. This is achieved by extending the realm of the MSF to topological signals [37]. To derive the higher-order MSF, we linearize the dynamical equation (7) by writing $\boldsymbol{\phi} = \boldsymbol{\omega} \otimes \mathbf{1}_{N_n} + \delta\boldsymbol{\phi}$ and we project on the eigenbasis of the Hodge Laplacian $\mathbf{L}_{[n]}$, by obtaining

$$\frac{d\delta\boldsymbol{\phi}_\Lambda}{dt} = (\mathbf{J}_F(\boldsymbol{\omega}) - \Lambda\mathbf{J}_h(\boldsymbol{\omega}))\delta\boldsymbol{\phi}_\Lambda, \tag{10}$$

where $\Lambda = \Lambda_{[n]}$ is the generic eigenvalue of $\mathbf{L}_{[n]}$, $\mathbf{J}_F$ and $\mathbf{J}_h$ are the Jacobians of functions F and h, respectively, and $\delta\boldsymbol{\phi}_\Lambda$ is the component of $\delta\boldsymbol{\phi}$ along the eigenvector corresponding to the eigenvalue Λ. This system of ODEs parametrized by the eigenvalues $\Lambda_{[n]}$ constitutes the MSF for topological signals and allows us to infer the stability of the synchronized solution by considering the spectrum of the Hodge Laplacian $\mathbf{L}_{[n]}$.

We observe that higher-order topological signals conditions (9) necessary for observing GTS on unweighted simplicial complexes are very restrictive [37]. There authors proved that some unweighted topologies allow global synchronization of their topological signals regardless of their dimensions. These topological spaces include the square lattices (2D torus) and the cubic lattices (3D torus) with periodic boundary conditions. Other notable examples of simplicial and cell complexes admitting global synchronization of their n-order topological signals are arbitrary n-dimensional discrete manifolds.

Moreover, in Ref. [37] it was also proved that odd-dimensional topological signals can never synchronize on unweighted simplicial complexes of dimension $d > 1$.

The aim of this paper is to demonstrate that by considering weighted simplicial complexes, one can overcome this limitation and it is thus possible to observe GTS also for odd-dimensional topological signals on simplicial complexes as well. Specifically, we will provide evidence that two weighted simplicial complexes, the WTT and the WW can sustain global synchronization of the edge signal given the appropriate choice of the edge weights.

IV. THE WEIGHTED TRIANGULATED TORUS AND THE WEIGHTED WAFFLE

The aim of this section is to discuss two examples of weighted simplicial complexes that allow global topological synchronization of the edge topological signals: the WTT and the WW. The WTT is formed by a square lattice with periodic boundary conditions where each square is triangulated forming a regular lattice in which each node has degree 6, and we are thus dealing with a triangulation of a 2D torus. In Fig. 1, we schematically show the WTT, the convention used for the orientation of its edges and triangles, and the notation adopted to indicate the different weights of the three distinct types of edges of this simplicial complex. According to the theory hereby presented, the edge signal admits a GTS on the WTT as long as the following condition is satisfied:

$$\mathbf{L}_{[n]}\mathbf{u} = 0, \tag{11}$$

with $\mathbf{u}$ the vector of elements of constant absolute value. Because of the Hodge decomposition, the latter rewrites

$$\mathcal{B}_{[n]}\mathbf{u} = \mathbf{0}, \quad \mathcal{B}^\top_{[n+1]}\mathbf{u} = \mathbf{0}. \tag{12}$$

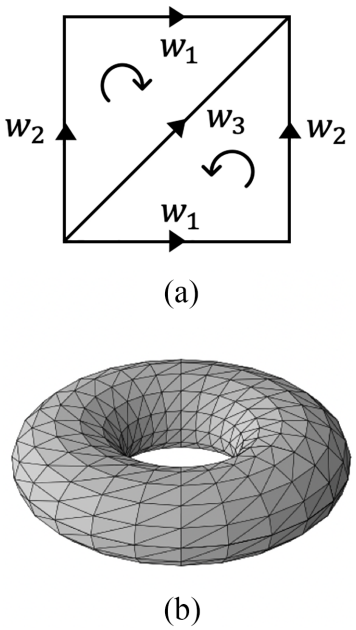

FIG. 1. The weighted triangulated torus (WTT) is a two-dimensional simplicial complex constructed from a square lattice with periodic boundary conditions. In this lattice, each periodic (square) unit is triangulated, thus the network skeleton of the simplicial complex is a regular lattice in which each node has degree 6. (a) Periodic (square) unit indicating the edge weights and their orientations (arrow), together with the two triangles and their orientations (circular arrows). (b) Three-dimensional view of the WTT.

We assume $\mathbf{G}_{[0]} = \mathbf{I}_{N_0}$ and $\mathbf{G}_{[2]} = \mathbf{I}_{N_2}$, namely, we do not consider weights on nodes and on faces, and we study the conditions on the edges weights w_α determining a nontrivial metric matrix $\mathbf{G}_{[1]}$ that guarantees GTS of the edge signals, i.e., it satisfies condition Eq. (11) for $n = 1$. On a WTT where each triangle is obtained from an identical triangulation or a rectangular lattice, the first of the conditions in Eqs. (12) can be easily satisfied as long as each rectangle is the same. The second condition in Eqs. (12) implies that the WTT only admits a global synchronized state of the edge signal if

$$\sqrt{\frac{1}{w_1}} + \sqrt{\frac{1}{w_2}} = \sqrt{\frac{1}{w_3}}, \tag{13}$$

where the edge weights $w_1, w_2, w_3 \in \mathbb{R}^+$ are defined in Fig. 1 and are independent of the edge direction. We refer the interested reader to Appendix A for the derivation of the latter condition.

This global synchronized state for the edges will be stable under appropriate dynamical conditions determined by the topological MSF. In Appendix B, we show the detailed derivation of the spectrum of the $\mathbf{L}_{[0]}$, $\mathbf{L}_{[1]}$, and $\mathbf{L}_{[2]}$ Hodge Laplacians. We note that the constant eigenvector $\mathbf{u} = \mathbf{1}_{N_0}$ is in the kernel of $\mathbf{L}_{[0]}$ and the constant eigenvector $\mathbf{u} = \mathbf{1}_{N_2}$ is in the kernel of $\mathbf{L}_{[2]}$. While the constant eigenvector $\mathbf{u} = \mathbf{1}_{N_1}$ is in the kernel of $\mathbf{L}_{[1]}$ only the provided Eq. (13) is satisfied. The spectra of the n-Hodge Laplacian of the WTT can significantly vary as a function of the chosen weights w_1 and w_2, even if we consider exclusively choices of w_3 satisfying Eq. (13). To

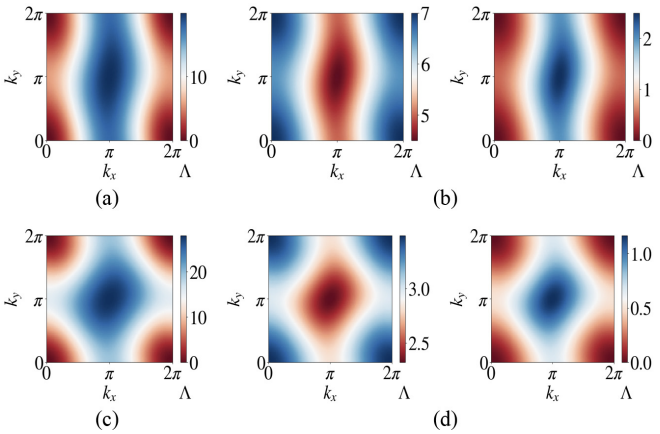

FIG. 2. The spectra of the weighted Hodge Laplacians $L^{\text{down}}_{[1]}$, $L^{\text{up}}_{[1]}$, coinciding with the spectra of $L_{[0]}$ and $L^{\text{down}}_{[2]}$, respectively, are reported for WTTs. Note that the $L^{\text{down}}_{[1]}$ spectrum consists of one band, while the $L^{\text{up}}_{[1]}$ spectrum consists of two bands. These spectra determine the values of the eigenvalues Λ of the $L^{\text{down}}_{[1]}$ [(a), (c)] and of the $L^{\text{up}}_{[1]}$ [(b), (d)] Laplacians as a function of the wave number $\mathbf{k} = (k_x, k_y)$. (a), (b) WTT with edge weights $w_1 = 1$, $w_2 = 4$, $w_3 = \frac{4}{9}$; (b), (d) WTT with edge weights $w_1 = 3$, $w_2 = 4$, $w_3 = \frac{36}{(2\sqrt{3}+3)^2}$.

demonstrate this phenomenon, in Fig. 2 we show the spectrum of $\mathbf{L}_{[0]}$ (coinciding with the nonzero spectrum of $\mathbf{L}^{\text{down}}_{[1]}$) and the two-band spectrum of $\mathbf{L}^{\text{down}}_{[2]}$ (coinciding with the nonzero spectrum of $\mathbf{L}^{\text{up}}_{[1]}$) for different values of the weights w_1 and w_2. For the analytical derivation of these spectra, we refer to Appendix B 1.

We consider here a second example of weighted simplicial complex that under suitable condition can also sustain GTS for edge signals: the WW. This is a three-dimensional simplicial complex whose building blocks (unit cells) are tetrahedra glued together along well-chosen edges. The edges joining different tetrahedra form a two-dimensional square lattice with periodic boundary conditions. In other words, the WW is a two-dimensional square lattice with periodic boundary conditions (torus) where each square of the lattice is substituted by a tetrahedron. In Fig. 3, we schematically show the WW together with the used convention for the orientation of its edges, triangular faces, and the notation adopted to indicate the different weights of the four distinct types of edges. Also, in this case, we assume $\mathbf{G}_{[0]} = \mathbf{I}_{N_0}$ and $\mathbf{G}_{[2]} = \mathbf{I}_{N_2}$ and study the conditions on the edges weights, w_α, determining a nontrivial metric matrix $\mathbf{G}_{[1]}$ that guarantees GTS of the edge signals, i.e., it satisfies condition Eq. (11) for $n = 1$. For the case of the WW, these conditions read

$$\sqrt{\frac{1}{w_3}} = \sqrt{\frac{1}{w_1}} + \sqrt{\frac{1}{w_2}},$$
$$\sqrt{\frac{1}{w_4}} = \sqrt{\frac{1}{w_1}} - \sqrt{\frac{1}{w_2}}, \tag{14}$$

where the edge weights $w_1, w_2, w_3, w_4 \in \mathbb{R}^+$ are defined in Fig. 3 and are independent of the edge direction. We refer to Appendix B for a detailed derivation of the spectrum of

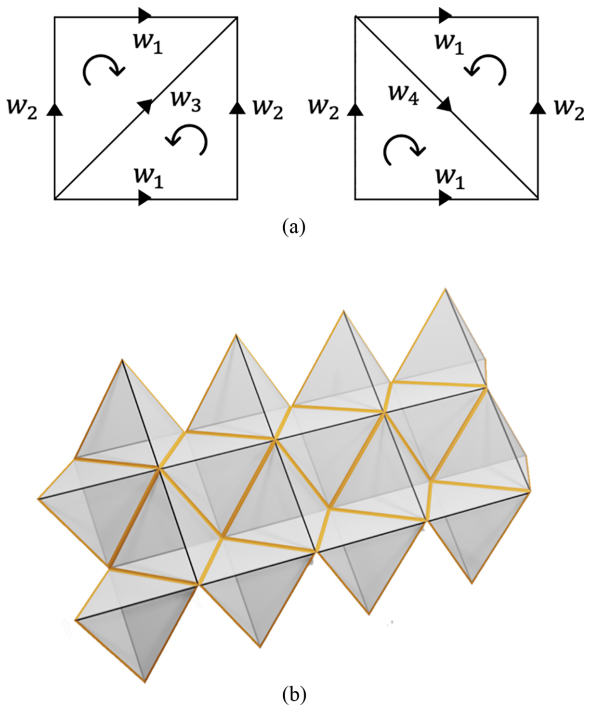

FIG. 3. The weighted waffle (WW) is a three-dimensional simplicial complex that can be constructed from a square lattice with periodic boundary conditions by substituting each square with a tetrahedron. In this lattice, each periodic unit is a tetrahedron, sharing four edges with the neighbor tetrahedra. In (a), we report the periodic (square) unit indicating the edge weights and their orientation (arrow), together with the two triangles and their orientations (circular arrows). (b) Three-dimensional view of the WW.

the $\mathbf{L}_{[0]}$, $\mathbf{L}_{[1]}$, and $\mathbf{L}_{[2]}$ Hodge Laplacians. We note that the constant eigenvector $\mathbf{u} = \mathbf{1}_{N_0}$ is in the kernel of $\mathbf{L}_{[0]}$ and the constant eigenvector $\mathbf{u} = \mathbf{1}_{N_2}$ is in the kernel of $\mathbf{L}_{[2]}$. The constant eigenvector $\mathbf{u} = \mathbf{1}_{N_1}$ is in the kernel of $\mathbf{L}_{[1]}$ only provided conditions (14) are satisfied. The spectra of the n-Hodge Laplacian of the WWs can vary significantly as a function of the choice adopted for the weights w_1 and w_2, also if we consider exclusively choices of w_3 and w_4 satisfying Eqs. (14). To demonstrate this phenomena in Fig. 4, we plot the spectrum of $\mathbf{L}_{[0]}$ (coinciding with the nonzero spectrum of $\mathbf{L}^{\text{down}}_{[1]}$) and the three nontrivial band spectrum of $\mathbf{L}^{\text{down}}_{[2]}$ (coinciding with the nonzero spectrum of $\mathbf{L}^{\text{up}}_{[1]}$) for different values of weights w_1 and w_2 and values of weights w_3 and w_4 determined by Eqs. (14).

V. GLOBAL TOPOLOGICAL SYNCHRONIZATION OF EDGE SIGNALS

In this section, we provide evidence that weighted simplicial complexes can sustain GTS of odd-dimensional signals. Specifically, we consider the Stuart-Landau (SL) model for global synchronization of topological signals. The Stuart-Landau (also known as the complex Ginzburg-Landau equation) is a paradigmatic model for the study of synchronization because it is the normal form of the supercritical Hopf-Andronov bifurcation [70]. This means that every oscillatory system

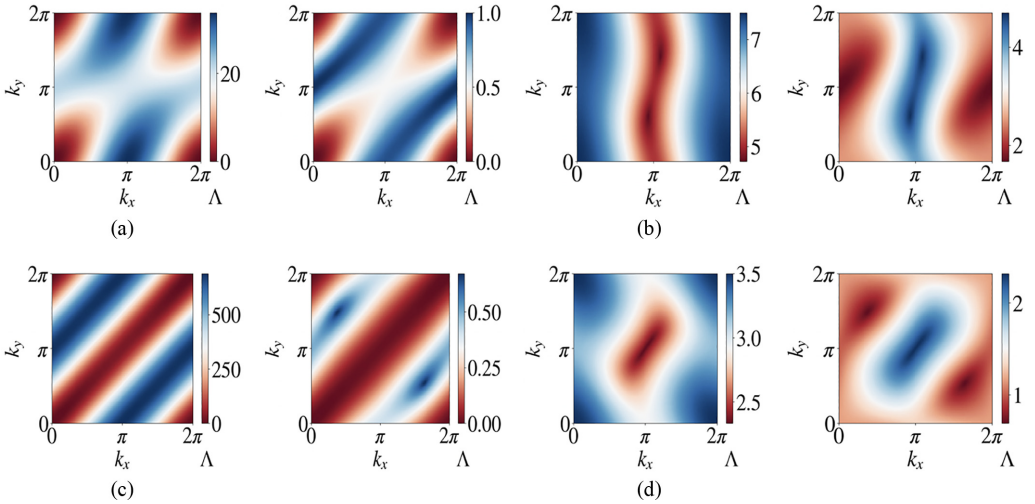

FIG. 4. The spectra of the weighted Hodge Laplacians $L_{[1]}^{\text{down}}$, $L_{[1]}^{\text{up}}$, coinciding with the spectra of $L_{[0]}$ and $L_{[2]}^{\text{down}}$, respectively, are reported for WWs. Note that $L_{[1]}^{\text{down}}$ spectrum consists of one band, while the $L_{[1]}^{\text{up}}$ spectrum consists of three nontrivial bands. These spectra determine the values of the eigenvalues Λ of the $L_{[1]}^{\text{down}}$ [(a), (c)] and $L_{[1]}^{\text{up}}$ [(b), (d)] Laplacians as a function of the wave-number $\mathbf{k} = (k_x, k_y)$. (a), (b) WW with edge weights $w_1 = 1$, $w_2 = 4$, $w_3 = \frac{4}{9}$, $w_4 = 4$; (b), (d) WW with edge weights $w_1 = 3$, $w_2 = 4$, $w_3 = \frac{36}{(2\sqrt{3}+3)^2}$, $w_4 = \frac{36}{(2\sqrt{3}-3)^2}$.

behaves like a Stuart-Landau oscillator close to such bifurcation and, in fact, can be reduced to a Stuart-Landau through the center-manifold reduction [71]. In this model, the elements of the n-cochain $\boldsymbol{\phi}$ are complex valued, i.e., $\phi_\alpha = \omega \in \mathbb{C}$. The functions $F(\omega)$ and $h(\omega)$ are taken to be $F(\omega) = \delta\omega - \mu|\omega|^2\omega$, $h(\omega) = \omega|\omega|^{m-1}$, where $\delta, \mu \in \mathbb{C}$, and $m \in \mathbb{N}$ are parameters of the model. Note that these functions are odd, therefore this choice allows us to define an equivariant dynamical equation for global topological synchronization.

The uncoupled system $\dot{\boldsymbol{\phi}} = \mathbf{F}(\boldsymbol{\phi})$ leads to identical equations involving each one a single simplex and reads $\dot{\omega} = F(\omega)$. This equation admits a limit cycle solution $\omega^{LC}(t) = \sqrt{\text{Re}(\delta)/\text{Re}(\mu)}e^{i2\pi ft}$, where the frequency of the oscillation obeys $2\pi f = \text{Im}(\delta) - \text{Im}(\mu)\text{Re}(\delta)/\text{Re}(\mu)$; moreover, the limit cycle is stable provided $\text{Re}(\delta) > 0$ and $\text{Re}(\mu) > 0$, conditions that we hereby assume to hold true.

In Figs. 5(a) and 5(c), we report numerical evidence for the GTS of edge signals associated to SL defined on the WTT whose weights satisfy Eq. (13); Figs. 5(b) and 5(d) refer to SL defined on the WW whose weights satisfy Eqs. (14). In both cases, we have considered parameters δ and μ which ensure the existence of a stable limit cycle according to the conditions given by the MSF. The achievement of the GTS state is revealed by the (generalized) Kuramoto order parameter R given by

$$R = \frac{1}{N_1}\sum_{\alpha\in Q_1}\rho_\alpha(t)e^{i\theta_\alpha}, \tag{15}$$

where we have rewritten the complex edge signal in polar coordinates, $\omega_\alpha = \rho_\alpha e^{i\theta_\alpha}$, with $\rho_\alpha, \theta_\alpha \in \mathbb{R}$. Let us recall that Q_1 indicates the set of all the one-dimensional simplices of the simplicial complex under study.

The order parameter R displays a fast convergence to one, indicating that $\rho_\alpha(t) \to 1$ and $\theta_\alpha(t) - \theta_{\alpha'}(t) \to 0$ for all α, α', thus testifying the emergence of GTS [see Fig. 5(a) for WTT and Fig. 5(b) for WW]. Additional evidence of GTS is shown in Figs. 5(c) and in 5(d), displaying temporal snapshots of the real part of the edge topological signals after a transient interval of time—the presence of vertical stripes is a signature of GTS, being the values assumed by the variable identical across all the link for any fixed time.

VI. GEOMETRICAL INTERPRETATION OF THE WEIGHTS

A. Geometrical interpretation of the weights on flat simplices

Considering theoretical frameworks [51] based on the HagenPoiseuille's equation in fluid dynamics and generalizing them to higher dimension,s the weight w_α associated to

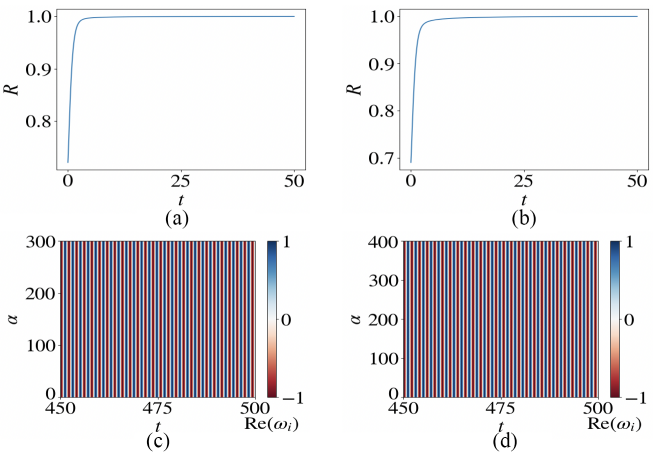

FIG. 5. Numerical evidence for GTS on the WTT [(a), (c)] and on the WW [(b), (d)]. (a), (b) Generalized order parameter $R(t)$ during the transient evolution showing the fast convergence to 1. (c), (d) Temporal evolution of the real part of the edge topological signal after a transient interval, namely, once it has reached its asymptotic state. The edge weights are $w_1 = 1$, $w_2 = 4$, $w_3 = \frac{4}{9}$ for the WTT, and $w_1 = 1$, $w_2 = 4$, $w_3 = \frac{4}{9}$, $w_4 = 4$ for the WW. For both simplicial complexes, the SL model parameters are given by $\delta = 1 + 4.3\text{i}$, $\mu = 1 + 1.1\text{i}$, $\sigma = 1 - 0.5\text{i}$, $m = 3$.

simplex α can be expressed as

$$w_\alpha = \frac{c_\alpha}{\ell_\alpha}, \tag{16}$$

where $c_\alpha \in \mathbb{R}^+$ is the *capacitance* associated to simplex α and ℓ_α is associated to the *volume* of simplex α. The volume of simplex ℓ_α is given for one-dimensional simplices by the length of the edges and for two-dimensional simplices by the area of the polygons, and so on for higher-order simplices. Here we focus, in particular, on the edges of the simplicial complex and investigate under which conditions the assumption that guarantees that a simplicial complex can sustain GTS admits a geometrical interpretation. When there are no constraints on the capacitance associated to the edges, the question is trivial, as the capacitances can always be tuned in such a way as to match the weights of the edges for any arbitrary distribution of their lengths. Nevertheless, if we impose that the capacitances are all equal, i.e., if we set

$$\ell_\alpha = \varphi\left(\frac{1}{\sqrt{w_\alpha}}\right) \tag{17}$$

for some smooth function φ, the problem becomes much harder. We thus here investigate the geometrical conditions under which conditions in Eq. (13) are satisfied if the weights are given by the inverse of the distance of the edges (i.e., if all the capacitances are set to one, $c_\alpha = 1$). For the sake of pedagogy, let us first assume $\varphi(x) = x$, hence Eq. (13) rewrites

$$\sqrt{\ell_1} + \sqrt{\ell_2} = \sqrt{\ell_3}. \tag{18}$$

Assuming the metric to be Euclidean, for Pythagoras's theorem we have

$$\ell_3^2 = \ell_1^2 + \ell_2^2 - 2\ell_1\ell_2 \cos\gamma_{12}, \tag{19}$$

where γ_{12} indicates the angle between edge ℓ_1 and edge ℓ_2. Equations (18) and (19) can be rewritten as

$$\begin{aligned} y_1 + y_2 &= 1, \\ y_1^4 + y_2^4 - 2y_1^2y_2^2\cos\gamma_{12} &= 1, \end{aligned} \tag{20}$$

where $y_1 = \sqrt{\ell_1/\ell_3}$, $y_2 = \sqrt{\ell_2/\ell_3}$. This system of equations leads to the only real solution given by the trivial (unphysical ones) $(y_1, y_2) = (1, 0)$, $(y_1, y_2) = (0, 1)$. It follows that if all the capacitances are equal, condition Eq. (13) is not compatible with a geometrical interpretation of the edge weights, as long as the simplices are flat Euclidean simplices.

B. Curved simplices

To tackle the above limitation, we investigate in this section whether curved simplices can allow us to gain a geometrical interpretation of the edge weights. Specifically, we will consider the case of the constraint Eq. (13) that guarantees the existence of a GTS state for the edge signal of the two-dimensional WTT. We indicate with ℓ_1 and ℓ_2 the lengths of the rectangular lattice tessellating the torus and assume that edges that have been inserted to triangulate the torus, i.e., those with weight w_3 in Fig. 1, are curved [see Fig. 6(a)] and form an arc of ellipses parametrized by the curve

$$x(t) = \frac{\ell_1}{2}\cos t, \quad y(t) = \frac{\ell_2}{2}\cos t, \quad z(t) = A\sin t,$$

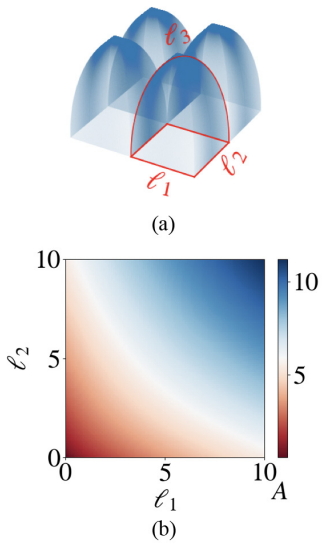

FIG. 6. (a) The geometrical realization of the WTT with curved simplices. Relationships between the length A of the curved edge of weight w_3 as a function of length ℓ_1, and ℓ_2 of the edges with weight w_1 and w_2 (b) in the geometrical realization of the WTT.

with $t \in [0, \pi]$. The value of A indicating the maximum height of the arc of the ellipse is determined by imposing that the length of the arc is $\ell_3 = (\sqrt{\ell_1} + \sqrt{\ell_2})^2$, i.e.,

$$\begin{aligned} \ell_3 = (\sqrt{\ell_1} + \sqrt{\ell_2})^2 &= \int_0^\pi \sqrt{\frac{\ell_1^2 + \ell_2^2}{4}\sin^2 t + A^2\cos^2 t}\,dt \\ &= \frac{1}{2}\sqrt{\ell_1^2 + \ell_2^2}\,E\left(1 - \frac{4A^2}{\ell_1^2 + \ell_2^2}\right) + AE\left(1 - \frac{\ell_1^2 + \ell_2^2}{4A^2}\right), \end{aligned}$$

where $E(m)$ indicates here the elliptic integral, i.e., $E(m) = \int_0^{\pi/2}\sqrt{1 - m\sin^2\theta}\,d\theta$.

This equation can be solved numerically; in Fig. 6(b), we show the dependence of A on ℓ_1 and ℓ_2.

Thus, in the case of the two-dimensional WTT, condition Eq. (13) can be geometrically interpreted by considering curved simplices. Note, however, that this construction is not generalizable to the WW.

C. Beyond the case $\varphi(x) = x$

An interesting question is whether we can gain a geometrical interpretation of the weights guaranteeing global topological synchronization of the edge signal if we relax the preliminary assumption $\varphi(x) = x$ and assume a more general functional dependence relating the length of the edges ℓ_α with their weights w_α. Let us observe that, under the assumption of flat simplices, the function φ is constrained to satisfy the triangular inequality (see Appendix C for details). In the case of the WTT, we can prove that if $\varphi(x)$ is a subadditive function, i.e., if

$$\varphi(x_1 + x_2) < \varphi(x_1) + \varphi(x_x), \tag{21}$$

then the triangular inequality is satisfied and thus Eq. (13) is compatible with the triangular inequality (see Theorem 1 in Appendix C).

Examples of functions in this class are, for instance,

$$\varphi(x) = x^{2\beta}, \tag{22}$$

with $2\beta < 1$ and

$$\varphi(x) = 1 - e^{-x}. \tag{23}$$

In the case of the WW, the problem is more complicated, as we need to check whether both constraints in Eqs. (14) are compatible with the triangular inequality once we assume that the lengths are related to the weights of the edges according to Eq. (17). As we show in Appendix C 2, this latter problem has no solution. In other words, there is no function $\varphi(x)$ that is compatible with the triangular inequality and satisfies both Eqs. (14).

VII. CONCLUSION

Weighted simplicial complexes can allow for the synchronization of topological signals even when their unweighted counterpart does not. Indeed, weights can be tuned in such a way to change the spectral properties of the simplicial complex and allow a constant eigenvector (or an eigenvector with constant absolute value of its elements) to lie in the kernel of the weighted Hodge Laplacians. Specifically, despite that odd-dimensional topological signals can never globally synchronize on unweighted simplicial complexes, we here provided two examples of weighted simplicial complexes that can sustain global synchronization of odd-dimensional topological signals (edge signal) provided suitable conditions on their edge weights are met. We provided an insightful description of these two weighted simplicial complexes, the WTT and WW, fully characterizing their higher-order spectral properties. We have shown that these two weighted simplicial complexes can sustain global synchronization of edge signals in the framework of the higher-order Stuart-Landau model. Moreover, we have investigated the possible geometric interpretation of the constraints necessary to observe global synchronization. Our findings reveal that global synchronization of odd-dimensional signals can be observed on simplicial complexes, provided suitable constraints of their weights are met. However, in the general scenario, these constraints on the weights do not have a simple and direct geometrical interpretation.

ACKNOWLEDGMENTS

The authors are grateful to L. Giambagli for discussions and feedback. R.M. acknowledges JSPS KAKENHI No. JP22K11919, No. JP22H00516, and JST CREST JPMJCR1913 for financial support.

APPENDIX A: DERIVATION OF NECESSARY CONDITIONS TO HAVE $\mathbf{u} \in \ker \mathbf{L}_{[n]}$

The aim of this Appendix is to develop the computations required to determine the conditions on the edges weights to have $\mathbf{u} \in \ker \mathbf{L}_{[n]}$, where $\mathbf{u} = (1, \ldots, 1)^\top$, in the case of the WTT, i.e., Eq. (13), and the WW, i.e., Eqs. (14).

Let us recall that in the case of unweighted simplicial complexes, the condition $\mathbf{B}_{[1]}\mathbf{u} = 0$ amounts to requiring that each node, i.e., entry in the vector $\mathbf{B}_{[1]}\mathbf{u}$, has as many incoming as outgoing edges by taking into account the orientation of the latter. Once weights are taken into account, that is, the sum of incoming and outgoing weights from any node, that should vanish, where we associate signed weights by using the edge orientations.

The condition $\mathbf{B}_{[2]}^\top \mathbf{u} = 0$ is equivalent to require, in the unweighted case, that for any triangle the sum of the orientations of the edges forming the boundary of the triangle should vanish. One can easily realize that this condition is never met; indeed, any triangle contains three edges whose orientations can only be $+1$ or -1 and thus their sum is an odd number. By introducing weights, the sum of the signed weights should vanish, where signs are again assigned according to the orientation of the triangle and the edges. There are thus choices of weights that satisfy this condition, as we will show hereafter.

1. Weighted triangulated torus

Let us refer to Fig. 1(a), where one can realize the existence of two different kinds of nodes: the ones with degree 6, e.g., the one in the bottom left or top right position, and those with degree 4, e.g., the one in the bottom right or top left position. By direct inspection of the orientations and edge weights, we can conclude that for nodes of the first kind, each row of the matrix $\mathbf{B}_{[1]}\mathbf{G}_{[1]}^{-1/2}$ has only six nonzero entries given by $\pm\sqrt{w_1}$, $\pm\sqrt{w_2}$, and $\pm\sqrt{w_3}$. On the other hand, for nodes of the second kind, the matrix will only have four nonzero entries with values $\pm\sqrt{w_1}$ and $\pm\sqrt{w_2}$. Hence, $\mathbf{B}_{[1]}\mathbf{G}_{[1]}^{-1/2}\mathbf{u} = 0$.

Still referring to Fig. 1(a), we can consider one oriented triangle and its three boundary edges, also oriented; then it is straightforward to realize that each row of the matrix $\mathbf{B}_{[2]}^\top\mathbf{G}_{[1]}^{\top/2}$ has only three nonvanishing entries given by $1/\sqrt{w_1}$, $1/\sqrt{w_2}$, and $-1/\sqrt{w_3}$. Thus, condition $\mathbf{B}_{[2]}^\top\mathbf{G}_{[1]}^{\top/2}\mathbf{u} = 0$ can be satisfied if and only if $1/\sqrt{w_1} + 1/\sqrt{w_2} = 1/\sqrt{w_3}$, namely, Eq. (13).

2. Weighted waffle

Let us now consider the WW and use Fig. 3 to help the reader in the following analysis.

Each node of the WW has degree 8, hence each row of the matrix $\mathbf{B}_{[1]}\mathbf{G}_{[1]}^{-1/2}$ has only eight nonzero entries, given by $\pm\sqrt{w_1}$, $\pm\sqrt{w_2}$, and $\pm\sqrt{w_3}$ in the case of nodes a or c, and $\pm\sqrt{w_1}$, $\pm\sqrt{w_2}$, and $\pm\sqrt{w_4}$ in the case of nodes b or d [see Fig. 3(a)]. In any cases, it follows that $\mathbf{B}_{[1]}\mathbf{G}_{[1]}^{-1/2}\mathbf{u} = 0$.

Let us now consider the triangular faces. By looking at Fig. 8, one can realize that there are essentially two kinds of faces, A and B or C and D. Hence, each row of the matrix $\mathbf{B}_{[2]}^\top\mathbf{G}_{[1]}^{\top/2}$ corresponding to a face of kind A and B has only three nonvanishing entries given by $1/\sqrt{w_1}$, $1/\sqrt{w_2}$, and $-1/\sqrt{w_3}$, while rows associated to faces of kinds C and D have only three nonvanishing entries given by $-1/\sqrt{w_1}$, $1/\sqrt{w_2}$, and $1/\sqrt{w_4}$. Thus, the condition $\mathbf{B}_{[2]}^\top\mathbf{G}_{[1]}^{\top/2}\mathbf{u} = 0$ can be satisfied if and only if $\frac{1}{\sqrt{w_1}} + \frac{1}{\sqrt{w_2}} = \frac{1}{\sqrt{w_3}}$ and $\frac{1}{\sqrt{w_1}} - \frac{1}{\sqrt{w_2}} = \frac{1}{\sqrt{w_4}}$, namely, Eqs. (14).

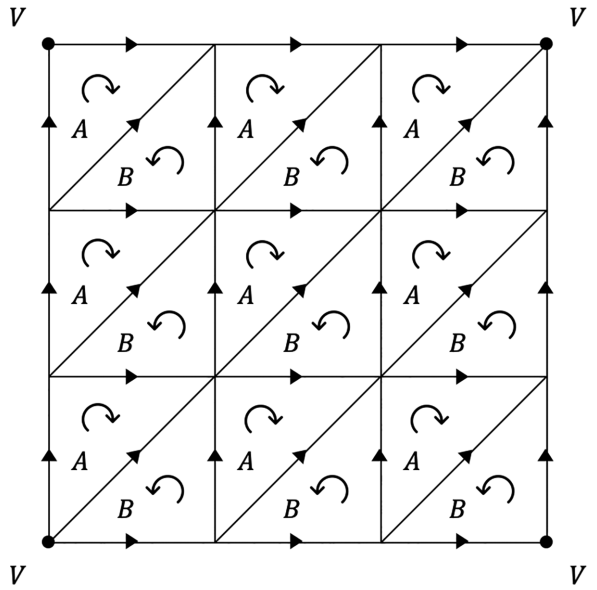

FIG. 7. Schematic representation of the WTT of linear size $\hat{L} = 3$ The unit cell of this simplicial complex is a square formed by two triangles of different types: type A and type B.

$$\left[\mathbf{L}^{\text{down}}_{[2]}\right]_{ij} = \begin{cases} \frac{1}{w_{[rs]}} + \frac{1}{w_{[rq]}} + \frac{1}{w_{[sq]}} & \text{if } i = j = [rsq] \\ \frac{1}{w_{[rs]}} & \text{if } i = [rsq],\ j = [rsq'],\ i \sim j \\ -\frac{1}{w_{[rs]}} & \text{if } i = [rsq],\ j = [rsq'],\ i \not\sim j, \end{cases}$$

where here we indicate with $i, j \in Q_2$ the generic triangles of the simplicial complex.

1. Spectrum of the weighted triangulated two-dimensional torus

We consider the weighted triangulated two-dimensional torus, namely, a two-dimensional simplicial complex formed by a triangulated 2D lattice with periodic boundary conditions and linear size $\hat{L}$ (for a schematic representation, see Fig. 7).

a. Spectrum of $\mathbf{L}_{[0]}$ *and* $\mathbf{L}^{down}_{[1]}$

Let us first calculate the spectrum of the 0-Hodge Laplacian $\mathbf{L}_{[0]}$ which coincides with the spectrum of the 1-down Hodge Laplacian $\mathbf{L}^{\text{down}}_{[1]}$. Due to the periodicity of the lattice, the wave number $\mathbf{k} = (k_x, k_y)$ has elements that take only the discrete values $k_x = \frac{2\pi n_x}{\hat{L}}$, and $k_y = \frac{2\pi n_y}{\hat{L}}$ with n_μ integer for $\mu \in \{x, y\}$ with $0 \leqslant n_x < \hat{L}$, $0 \leqslant n_y < \hat{L}$. We indicate the coordinates of each node j as $\mathbf{r}_j = (x_j, y_j)$ corresponding to the Cartesian coordinates of point j of the two-dimensional lattice. We indicate with $\mathbf{e}_x$ and $\mathbf{e}_y$ the unit vectors along the x and the y axis, respectively. Let us define $\mathbf{u} \in \mathbb{C}^{N_0}$ as the Fourier modes of the lattice; in other words, we take the components of $\mathbf{u}$ given by $[\mathbf{u}]_j = e^{i\mathbf{k}\cdot\mathbf{r}_j}$ with $\mathbf{k}\cdot\mathbf{r}_j = k_x x_j + k_y y_j$. Suppose that $\mathbf{u}$ is the eigenvector of the 0-Hodge Laplacian $\mathbf{L}_{[0]}$—here we want to find its corresponding eigenvalue $\Lambda_{[0]}$, i.e., we want to solve the eigenvalue problem:

$$\mathbf{L}_{[0]}\mathbf{u} = \Lambda_{[0]}\mathbf{u} \text{ with } [\mathbf{u}]_j = e^{i\mathbf{k}\cdot\mathbf{r}_j}. \tag{B2}$$

The jth entry of $\mathbf{L}_{[0]}\mathbf{u}$ is

$$\begin{aligned}
&[\mathbf{L}_{[0]}\mathbf{u}]_j \\
&= (2w_1 + 2w_2 + 2w_3)e^{i\mathbf{k}\cdot\mathbf{r}_j} - w_1[e^{i\mathbf{k}\cdot(\mathbf{r}_j-\mathbf{e}_x)} + e^{i\mathbf{k}\cdot(\mathbf{r}_j+\mathbf{e}_x)}] \\
&\quad - w_2[e^{i\mathbf{k}\cdot(\mathbf{r}_j-\mathbf{e}_y)} + e^{i\mathbf{k}\cdot(\mathbf{r}_j+\mathbf{e}_y}] - w_3\big[e^{i\mathbf{k}\cdot(\mathbf{r}_j-\mathbf{e}_x-\mathbf{e}_y)} \\
&\quad + e^{i\mathbf{k}\cdot(\mathbf{r}_j+\mathbf{e}_x+\mathbf{e}_y)}\big] \\
&= e^{i\mathbf{k}\cdot\mathbf{r}_j}\Bigg[4w_1 \sin^2\left(\frac{k_x}{2}\right) + 4w_2 \sin^2\left(\frac{k_y}{2}\right) \\
&\quad + 4w_3 \sin^2\left(\frac{k_x + k_y}{2}\right)\Bigg].
\end{aligned} \tag{B3}$$

Therefore, the eigenvalues $\Lambda_{[0]}$ of the 0-Hodge Laplacian $\mathbf{L}_{[0]}$ associated to the wave-number $\mathbf{k}$ are given by

$$\begin{aligned}
\Lambda_{[0]} &= 4w_1 \sin^2\left(\frac{k_x}{2}\right) + 4w_2 \sin^2\left(\frac{k_y}{2}\right) \\
&\quad + 4w_3 \sin^2\left(\frac{k_x + k_y}{2}\right).
\end{aligned} \tag{B4}$$

We note that $\Lambda_{[0]} = 0$ is an eigenvalue consistent with $\mathbf{k} = (0, 0)$ and $\mathbf{u} = \mathbf{1}_{N_0}$. Note that the nonzero eigenvalues $\Lambda_{[0]}$ of the 0-Hodge Laplacian $\mathbf{L}_{[0]}$ coincide with the nonzero eigenvalues $\Lambda_{[1]}$ of the Hodge Laplacian $\mathbf{L}^{\text{down}}_{[1]}$.

APPENDIX B: SPECTRUM OF THE CONSIDERED 2D-SIMPLICIAL COMPLEXES

The aim of this Appendix is to explicitly determine the spectra of the simplicial complexes studied in the main text, namely, the WTT and WW. Given the periodic nature of these simplicial complexes, we will adopt here an approach based on Bloch's theorem. Note that this approach cannot be adopted to study the spectra of aperiodic simplicial complexes for which different methods should be adopted (see, for instance, the renormalization methods used in Ref. [72]).

In the following, we will assume that the metric on the nodes and on the triangles are trivial and the only nontrivial metric matrix is the one associated to the edges. In this case, we recall that the elements of the $\mathbf{L}_{[0]}$ Laplacian are given by

$$[\mathbf{L}_{[0]}]_{ij} = \begin{cases} \sum_{r\in Q_0} w_{[ir]} & \text{if } i = j \\ -w_{[ij]}, & \text{if } i \neq j, \end{cases} \tag{B1}$$

where here we indicate with $i, j \in Q_0$ the generic nodes of the simplicial complex. Furthermore, the elements of the $\mathbf{L}^{\text{down}}_{[2]}$ Laplacian are given by

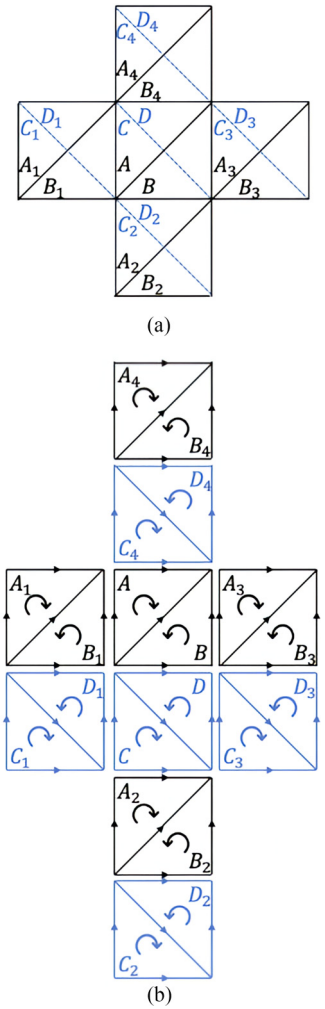

FIG. 8. Notation adopted for the WW. (a) A given tetrahedron of the WW whose faces are indicated according to their type (A, B, C, D) is visualized together with its four incident tetrahedra. We indicate in black the faces A, B pointing outward and in blue the faces C, D incident to the dashed blue line pointing inward (on the back). (b) represents the same five tetrahedra distinguishing between the faces pointing outward A, B and the faces pointing inward C, D. The orientation of the faces is also indicated, as this is important to derive the spectrum of the $\mathbf{L}_{[2]}^{\text{down}}$ Laplacian.

b. Spectrum of $L_{[1]}^{\text{up}}$ and $L_{[2]}^{\text{down}}$

The spectrum of 2-Hodge Laplacian $\mathbf{L}_{[2]}^{\text{down}} = \mathbf{B}_{[2]}^{\top}\mathbf{B}_{[2]}$ of the WTT coincides with the spectrum of the graph Laplacian of its dual hexagonal lattice. As indicated in Fig. 7, we distinguish between two different types of triangles (triangles of types A and B). The triangulated torus can be seen as a periodic lattice of cells (squares) j of coordinates $\mathbf{r_j} = (x_j, y_j)$, indicating the coordinate of their bottom-left node. Due to the periodicity of the lattice, we can use Bloch's theorem [73,74] and indicate the eigenvector $\mathbf{u} \in \mathbb{C}^{N_2}$ of the 2-down Hodge Laplacian $\mathbf{L}_{[2]}^{\text{down}}$ as

$$\mathbf{u}_i = e^{i\mathbf{k}\cdot\mathbf{r}_j}\begin{pmatrix} a_A \\ a_B \end{pmatrix}, \tag{B5}$$

where $a_A, a_B \in \mathbb{C}$ indicate the component of the eigenvector on the triangle of type A and type B, respectively. Due to the periodicity of the underlying square lattice, the wave numbers $\mathbf{k} = (k_x, k_y)$ have components that take only the discrete values $k_x = \frac{2\pi n_x}{\hat{L}}$, and $k_y = \frac{2\pi n_y}{\hat{L}}$ with n_μ integer for $\mu \in \{x, y\}$ with $0 \leqslant n_x < \hat{L}, 0 \leqslant n_y < \hat{L}$.

Given the choice of the parametrization of the eigenvector $\mathbf{u}$, we have

$$\begin{aligned}
&\left[\mathbf{L}_{[2]}^{\text{down}}\mathbf{u}\right]_{A,j} \\
&\quad = \left(\frac{1}{w_1} + \frac{1}{w_2} + \frac{1}{w_3}\right) a_A e^{i\mathbf{k}\cdot\mathbf{r}_j} \\
&\qquad - a_B\left[\frac{1}{w_1}e^{i\mathbf{k}\cdot(\mathbf{r}_j+\mathbf{e}_y)} + \frac{1}{w_2}e^{i\mathbf{k}\cdot(\mathbf{r}_j-\mathbf{e}_x)} + \frac{1}{w_3}e^{i\mathbf{k}\cdot\mathbf{r}_j}\right], \\
&\left[\mathbf{L}_{[2]}^{\text{down}}\mathbf{u}\right]_{B,j} \\
&\quad = \left(\frac{1}{w_1} + \frac{1}{w_2} + \frac{1}{w_3}\right) a_B e^{i\mathbf{k}\cdot\mathbf{r}_j} \\
&\qquad - a_A\left[\frac{1}{w_1}e^{i\mathbf{k}\cdot(\mathbf{r}_j-\mathbf{e}_y)} + \frac{1}{w_2}e^{i\mathbf{k}\cdot(\mathbf{r}_j+\mathbf{e}_x)} + \frac{1}{w_3}e^{i\mathbf{k}\cdot\mathbf{r}_j}\right].
\end{aligned} \tag{B6}$$

Thus, the eigenvalues $\Lambda_{[2]}$ of $\mathbf{L}_{[2]}^{\text{down}}$ form two bands, and for each choice the wave numbers $\mathbf{k} = (k_x, k_y)$ are given by

$$\Lambda_{[2]} = \frac{1}{w_1} + \frac{1}{w_2} + \frac{1}{w_3} \pm |f(\mathbf{k})|, \tag{B7}$$

where

$$f(\mathbf{k}) = \frac{1}{w_1}e^{i\mathbf{k}\cdot\mathbf{e}_y} + \frac{1}{w_2}e^{-i\mathbf{k}\cdot\mathbf{e}_x} + \frac{1}{w_3}, \tag{B8}$$

and thus

$$|f(\mathbf{k})| = \sqrt{\left(\frac{1}{w_1^2} + \frac{1}{w_2^2} + \frac{1}{w_3^2}\right) + \frac{2}{w_1 w_2 w_3}[w_1\cos(k_x) + w_2\cos(k_y) + w_3\cos(k_x + k_y)]}. \tag{B9}$$

We note that $\Lambda_{[2]} = 0$ is an eigenvalue consistent with $\mathbf{k} = (0, 0)$ and $a_A = a_B = 1$ consistent with $\mathbf{u} = \mathbf{1}_{N_2}$. The nonzero spectrum of the $\mathbf{L}_{[2]}^{\text{down}}$ given by nonzero eigenvalues $\Lambda_{[2]}$ coincides with the nonzero spectrum of $\mathbf{L}_{[1]}^{\text{up}}$ given by the eigenvalues $\Lambda_{[1]}$.

2. The spectrum of the WW

Here we determine the spectrum of the WW (see Fig. 8) by generalizing the approach used to derive the spectrum of the WTT. The WW is a periodic lattice of three-dimensional cells (tetrahedra) glued to each other along edges. Thus, the

edges incident to more than one tetrahedron form a regular square lattice of linear size $\hat{L}$. For this three-dimensional simplicial complex, we derive here the spectrum of the 0-Hodge Laplacian and the 1-Hodge Laplacian.

a. Spectrum of $\mathbf{L}_{[0]}$ *and* $\mathbf{L}_{[1]}^{\text{down}}$

We will first find the spectrum graph Laplacian of the WW. Using a similar technique as the one adopted for the WTT (see Sec. B 1 a), we obtain that the eigenvectors of the 0-Hodge Laplacian of the WW are given by the Fourier eigenmodes $\mathbf{u} \in \mathbb{C}^{N_0}$ of elements

$$[\mathbf{u}]_j = e^{i\mathbf{k}\cdot\mathbf{r}_j} \tag{B10}$$

associated to the wave numbers $\mathbf{k} = (k_x, k_y)$ with $k_x = \frac{2\pi n_x}{\hat{L}}$, and $k_y = \frac{2\pi n_y}{\hat{L}}$ where $0 \leqslant n_x < \hat{L}, 0 \leqslant n_y < \hat{L}$. The eigenvalues $\Lambda_{[0]}$ associated to these generic eigenvectors are

$$\Lambda_{[0]} = 4w_1 \sin^2\left(\frac{k_x}{2}\right) + 4w_2 \sin^2\left(\frac{k_y}{2}\right) + 4w_3 \sin^2\left(\frac{k_x - k_y}{2}\right) + 4w_4 \sin^2\left(\frac{k_x + k_y}{2}\right). \tag{B11}$$

We note that $\Lambda_{[0]} = 0$ is an eigenvalue consistent with $\mathbf{k} = (0, 0)$ and $\mathbf{u} = \mathbf{1}_{N_0}$. The nonzero spectrum of the 0-Hodge Laplacian $\mathbf{L}_{[0]}$ formed by the eigenvalues $\Lambda_{[0]}$ coincides with the nonzero spectrum of the 1-down Hodge Laplacian $\mathbf{L}_{[1]}^{\text{down}}$ formed by the eigenvalues $\Lambda_{[1]}$.

b. Spectrum of $L_{[1]}^{\text{up}}$ *and* $L_{[2]}^{\text{down}}$

The faces on each tetrahedron of the WW can be classified in four types: types *A,B,C*, and *D* (see Fig. 8). By using Bloch's theorem [73,74], the eigenvectors $\mathbf{u} \in \mathbb{C}^{N_2}$ of $\mathbf{L}_{[2]}^{\text{down}}$ have elements that for each tetrahedron i of coordinates $\mathbf{R}_i$ on the 2D torus having elements

$$\mathbf{u}_j = e^{i\mathbf{k}\cdot\mathbf{r}_j} \begin{pmatrix} a_A \\ a_B \\ a_C \\ a_D \end{pmatrix}, \tag{B12}$$

associated to the wave numbers $\mathbf{k} = (k_x, k_y)$ with $k_x = \frac{2\pi n_x}{\hat{L}}$, and $k_y = \frac{2\pi n_y}{\hat{L}}$ where $0 \leqslant n_x < \hat{L}, 0 \leqslant n_y < \hat{L}$. Here $a_A, a_B, a_C, a_D \in \mathbb{C}$ indicate the component relative to each of the four triangles of the tetrahedron forming each cell j. The Hodge Laplacian $\mathbf{L}_{[2]}^{\text{down}}$ couples each triangle to the other seven triangles sharing an edge of which three belong to the same tetrahedron, and the other four belong to the two adjacent tetrahedra of the triangular face (see Fig. 8). A direct calculation performed for the triangular faces of types A, B, C, and D leads to

$$\begin{aligned}
\left[\mathbf{L}_{[2]}^{\text{down}}\mathbf{u}\right]_{A,j} =& \left(\tfrac{1}{w_1} + \tfrac{1}{w_2} + \tfrac{1}{w_3}\right)a_A e^{i\mathbf{k}\cdot\mathbf{r}_j} + e^{i\mathbf{k}\cdot\mathbf{r}_j}\left[\tfrac{1}{w_3}a_B + \tfrac{1}{w_2}a_C - \tfrac{1}{w_1}a_D\right] \\
&+ e^{i\mathbf{k}\cdot(\mathbf{r}_j - \mathbf{e}_x)}\left[\tfrac{1}{w_2}(a_B + a_D)\right] + e^{i\mathbf{k}\cdot(\mathbf{r}_j + \mathbf{e}_y)}\left[\tfrac{1}{w_1}(a_B - a_C)\right], \\
\left[\mathbf{L}_{[2]}^{\text{down}}\mathbf{u}\right]_{B,j} =& \left(\tfrac{1}{w_1} + \tfrac{1}{w_2} + \tfrac{1}{w_3}\right)a_B e^{i\mathbf{k}\cdot\mathbf{r}_j} + e^{i\mathbf{k}\cdot\mathbf{r}_j}\left[\tfrac{1}{w_3}a_A - \tfrac{1}{w_1}a_C + \tfrac{1}{w_2}a_D\right] \\
&+ e^{i\mathbf{k}\cdot(\mathbf{r}_j + \mathbf{e}_x)}\left[\tfrac{1}{w_2}(a_A + a_C)\right] + e^{i\mathbf{k}\cdot(\mathbf{r}_j - \mathbf{e}_y)}\left[\tfrac{1}{w_1}(a_A - a_D)\right], \\
\left[\mathbf{L}_{[2]}^{\text{down}}\mathbf{u}\right]_{C,j} =& \left(\tfrac{1}{w_1} + \tfrac{1}{w_2} + \tfrac{1}{w_4}\right)a_C e^{i\mathbf{k}\cdot\mathbf{r}_j} + e^{i\mathbf{k}\cdot\mathbf{r}_j}\left[\tfrac{1}{w_2}a_A - \tfrac{1}{w_1}a_B + \tfrac{1}{w_4}a_D\right] \\
&+ e^{i\mathbf{k}\cdot(\mathbf{r}_j - \mathbf{e}_x)}\left[\tfrac{1}{w_2}(a_B + a_D)\right] + e^{i\mathbf{k}\cdot(\mathbf{r}_j - \mathbf{e}_y)}\left[\tfrac{1}{w_1}(-a_A + a_D)\right], \\
\left[\mathbf{L}_{[2]}^{\text{down}}\mathbf{u}\right]_{D,j} =& \left(\tfrac{1}{w_1} + \tfrac{1}{w_2} + \tfrac{1}{w_4}\right)a_D e^{i\mathbf{k}\cdot\mathbf{r}_j} + e^{i\mathbf{k}\cdot\mathbf{r}_j}\left[-\tfrac{1}{w_1}a_A + \tfrac{1}{w_2}a_B + \tfrac{1}{w_4}a_C\right] \\
&+ e^{i\mathbf{k}\cdot(\mathbf{r}_j + \mathbf{e}_x)}\left[\tfrac{1}{w_2}(a_A + a_C)\right] + e^{i\mathbf{k}\cdot(\mathbf{r}_j + \mathbf{e}_y)}\left[\tfrac{1}{w_1}(-a_B + a_C)\right].
\end{aligned} \tag{B13}$$

Thus, the spectrum of the $\mathbf{L}_{[2]}^{\text{down}}$ Hodge Laplacian comprises four bands having eigenvalues $\Lambda_{[2]}$ satisfying the eigenvalue problem

$$\mathcal{M}\begin{pmatrix} a_A \\ a_B \\ a_C \\ a_D \end{pmatrix} = \Lambda_{[2]}\begin{pmatrix} a_A \\ a_B \\ a_C \\ a_D \end{pmatrix}, \tag{B14}$$

where for each choice of wave number $\mathbf{k}$, matrix $\mathcal{M}$ is a 4×4 matrix given by

$$\mathcal{M} = \begin{pmatrix}
\frac{1}{w_1} + \frac{1}{w_2} + \frac{1}{w_3} & \frac{e^{ik_y}}{w_1} + \frac{e^{-ik_x}}{w_2} + \frac{1}{w_3} & -\frac{e^{ik_y}}{w_1} + \frac{1}{w_2} & -\frac{1}{w_1} + \frac{e^{-ik_x}}{w_2} \\
\frac{e^{-ik_y}}{w_1} + \frac{e^{ik_x}}{w_2} + \frac{1}{w_3} & \frac{1}{w_1} + \frac{1}{w_2} + \frac{1}{w_3} & -\frac{1}{w_1} + \frac{e^{ik_x}}{w_2} & -\frac{e^{-ik_y}}{w_1} + \frac{1}{w_2} \\
-\frac{e^{-ik_y}}{w_1} + \frac{1}{w_2} & -\frac{1}{w_1} + \frac{e^{-ik_x}}{w_2} & \frac{1}{w_1} + \frac{1}{w_2} + \frac{1}{w_4} & \frac{e^{-ik_y}}{w_1} + \frac{e^{-ik_x}}{w_2} + \frac{1}{w_4} \\
-\frac{1}{w_1} + \frac{e^{ik_x}}{w_2} & -\frac{e^{ik_y}}{w_1} + \frac{1}{w_2} & \frac{e^{ik_y}}{w_1} + \frac{e^{ik_x}}{w_2} + \frac{1}{w_4} & \frac{1}{w_1} + \frac{1}{w_2} + \frac{1}{w_4}
\end{pmatrix}. \tag{B15}$$

We note that $\Lambda_{[2]} = 0$ is an eigenvalue consistent with $\mathbf{k} = (0, 0)$ and $a_A = a_B = a_C = a_D = 1$ consistent with $\mathbf{u} = \mathbf{1}_{N_2}$. The nonzero spectrum of the $\mathbf{L}_{[2]}^{\text{down}}$ given by nonzero eigenvalues $\Lambda_{[2]}$ coincides with the nonzero spectrum of $\mathbf{L}_{[1]}^{\text{up}}$ given by the eigenvalues $\Lambda_{[1]}$. Additionally, we observe that although the spectrum of $\mathbf{L}_{[2]}^{\text{down}}$ is given by four bands, only three are nontrivial, as the eigenvalue corresponding to the fourth band is always null.

APPENDIX C: GEOMETRIC INTERPRETATION OF THE WEIGHTS: FURTHER MATHEMATICAL RESULTS

1. Weighted triangulated torus

The aim of this Appendix is to provide proof of the claim that using a subadditive function φ to relate edge weights and their lengths allows us to satisfy the triangular inequality.

We can indeed state

Theorem 1. Let $\varphi : \mathbb{R}_+ \to \mathbb{R}_+$ be a positive subadditive function vanishing only at zero. Then for any positive weights, w_1, w_2, and w_3 such that Eq. (13) holds true, the choice of lengths given by

$$\ell_j = \varphi\left(\frac{1}{\sqrt{w_j}}\right) \tag{C1}$$

satisfies the triangular inequality

Proof. By Eq. (13), we have

$$\frac{1}{\sqrt{w_3}} = \frac{1}{\sqrt{w_1}} + \frac{1}{\sqrt{w_2}};$$

hence by using the edge between weights and lengths, we get

$$\ell_3 = \varphi\left(\frac{1}{\sqrt{w_3}}\right) = \varphi\left(\frac{1}{\sqrt{w_1}} + \frac{1}{\sqrt{w_2}}\right). \tag{C2}$$

By using the subadditivity of φ, we have

$$\ell_3 < \varphi\left(\frac{1}{\sqrt{w_1}}\right) + \varphi\left(\frac{1}{\sqrt{w_2}}\right) = \ell_1 + \ell_2. \tag{C3}$$

■

A necessary and sufficient condition to have a positive smooth subadditive function is given by the following proposition:

Proposition 1. Let $\varphi : \mathbb{R}_+ \to \mathbb{R}_+$ be a differentiable, positive function vanishing at zero. Then φ is subadditive if and only if its first derivative is strictly monotone decreasing, namely, φ is strictly concave.

Proof. By using the smoothness of φ, for any $x > 0$ and $y > 0$ we can write

$$\varphi(x + y) - \varphi(y) = \int_y^{x+y} \varphi'(t)\, dt = \int_0^x \varphi'(t + y)\, dt,$$

and, similarly, by recalling the $\varphi(0) = 0$, we get

$$\varphi(x) = \int_0^x \varphi'(t)\, dt.$$

Hence

$$\begin{aligned}\varphi(x + y) - \varphi(y) - \varphi(x) &= \int_y^{x+y} \varphi'(t)\, dt - \int_0^x \varphi'(t)\, dt \\ &= \int_0^x [\varphi'(t + y) - \varphi'(t)]\, dt \\ &= \int_0^x dt \int_t^{t+y} \varphi''(s)\, ds. \end{aligned} \tag{C4}$$

Thus, the conclusion follows by remarking that a smooth strictly concave function satisfies $\varphi''(s) < 0$ for all s. ■

Example 1. The function $\varphi(t) = t^a$ is subadditive if and only if $0 < a < 1$. Indeed φ is smooth, positive, and vanishing at 0. Moreover, $\varphi'(t) = at^{a-1}$ and $\varphi''(t) = a(a - 1)t^{a-2}$; the latter is negative (for positive t) if and only if $0 < a < 1$. We can then apply the previous proposition. This shows the necessity to have $\beta < 1/2$.

Example 2. By using Proposition 1, we can obtain other interesting edges between weights and lengths, for instance,

$$\ell_j = 1 - e^{-1/\sqrt{w_j}}$$

does satisfy the triangular inequality.

Indeed, the smooth function $\varphi(t) = 1 - e^{-t}$ vanishes at zero and is positive for positive t. Moreover, its derivative $\varphi'(t) = e^{-t}$ is strictly monotone decreasing, hence $\varphi(t)$ is subadditive. In conclusion,

$$\begin{aligned}\ell_3 &= 1 - e^{-1/\sqrt{w_3}} = 1 - e^{-(1/\sqrt{w_1}+1/\sqrt{w_2})} \\ &< 1 - e^{-1/\sqrt{w_1}} + 1 - e^{-1/\sqrt{w_2}} = \ell_1 + \ell_2. \end{aligned} \tag{C5}$$

2. Weighted waffle

The starting point is the conditions given by Eqs. (14). Then, assuming again the existence of a relation among weights and lengths of the form $\ell_i = g(1/w_i)$, the previous conditions imply that:

(1) ℓ_1 is the longest side of the triangle whose sides are ℓ_1, ℓ_2, and ℓ_4; thus $\ell_1 > \ell_2$ and $\ell_1 > \ell_4$;

(2) the previous point implies that ℓ_1 must satisfies $\ell_1 < \ell_2 + \ell_4$;

(3) ℓ_3 is the longest side of the triangle whose sides are ℓ_1, ℓ_2 and ℓ_3, thus $\ell_3 > \ell_1$ and $\ell_3 > \ell_2$. Hence by the first point we have: $\ell_3 > \ell_1 > \ell_2$; and

(4) the previous point implies that ℓ_3 must satisfies $\ell_3 < \ell_1 + \ell_2$.

The aim of this section is to show that the previous conditions are not sufficient to define a tetrahedron, indeed by assuming to fix ℓ_1, ℓ_2, and ℓ_4, such that points 1 and 2 are satisfied, then ℓ_3 should belong to a well-defined interval, whose bounds depend on ℓ_1, ℓ_2, and ℓ_4 (and this allows us to automatically satisfy points 3 and 4).

To determine such bounds, let us consider Fig. 9. In Fig. 9(a), we show one face of the tetrahedron, i.e., the triangle with vertexes a, c, and d and sides of length ℓ_1 (green one), ℓ_2 (blue one), and ℓ_4 (red one). We assume this triangle to lie on the plane x, y and its vertexes to have coordinates $a = (\ell_4/2, 0)$, $c = (-\ell_4/2, 0)$, and $d(p, q)$, where one easily can obtain that

$$\ell_1^2 = \left(\frac{\ell_4}{2} + p\right)^2 + q^2 \text{ and } \ell_2^2 = \left(p - \frac{\ell_4}{2}\right)^2 + q^2,$$

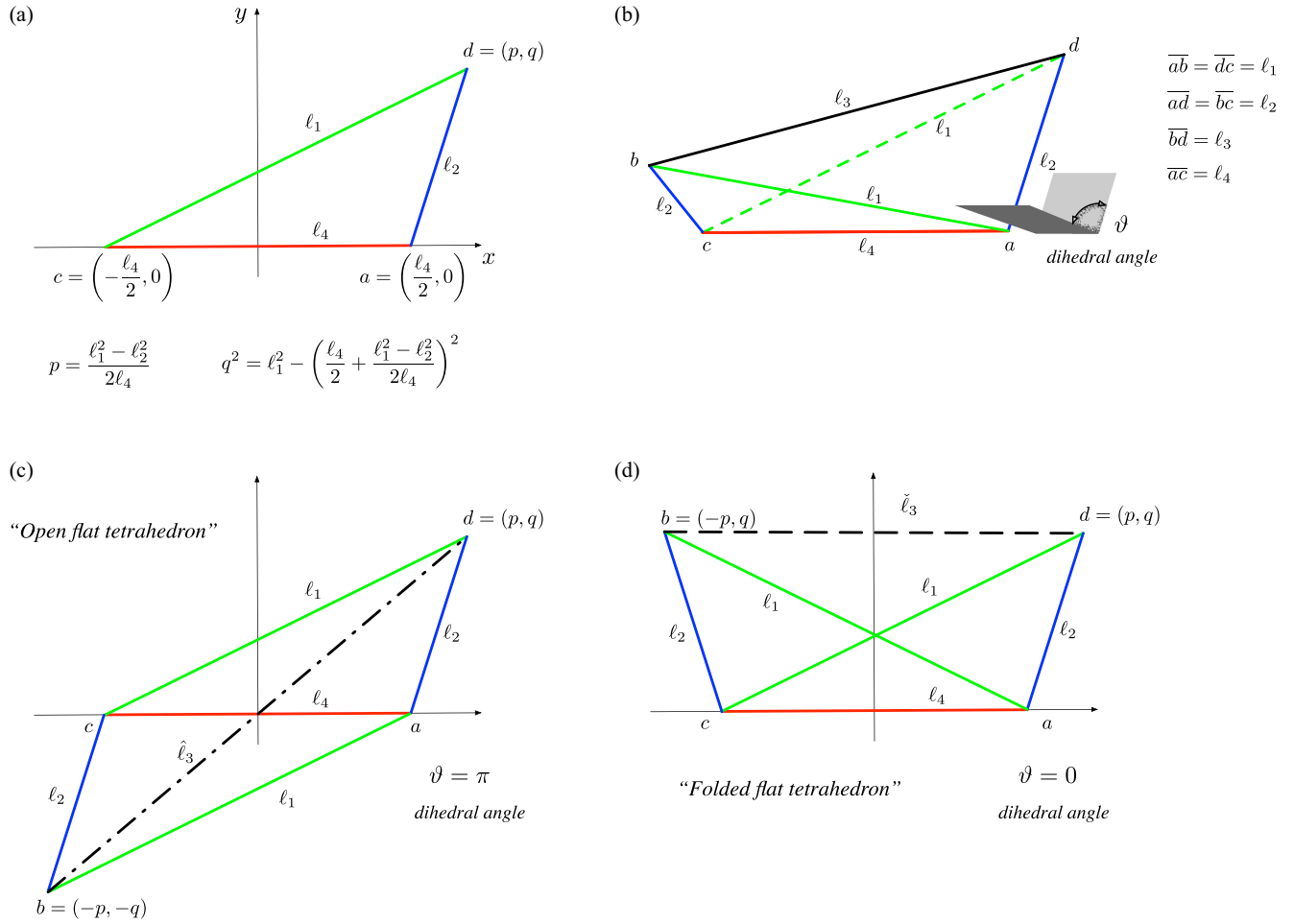

FIG. 9. Different views of the tetrahedron and its faces. Panel (a) presents one face of the tetrahedron, i.e., a triangle, in the coordinates plane (x, y) and their link with the sides lengths, ℓ_j, $j \in \{1, 2, 3, 4\}$. Panel (b) shows a 3D view of the tetrahedron, the dihedral angle, θ, formed by the faces $[abc]$ and $[acd]$, and the associated edges lengths. Panel (c) depicts a special "flat" tetrahedron where the faces $[abc]$ and $[acd]$ lie on the same plane, i.e., $\theta = \pi$. Panel (d) depicts a second special "flat" tetrahedron where the faces $[abc]$ and $[acd]$ lie again on the same plane but $\theta = 0$.

from which it follows:

$$p = \frac{\ell_1^2 - \ell_2^2}{2\ell_4} \text{ and } q^2 = \ell_1^2 - \left(\frac{\ell_4}{2} + \frac{\ell_1^2 - \ell_2^2}{2\ell_4}\right)^2. \tag{C6}$$

Let us now consider the full tetrahedron [Fig. 9(b)] obtained by gluing two triangles with sides ℓ_1, ℓ_2, and ℓ_4 along the latter side, and two triangles with sides ℓ_1, ℓ_2, and ℓ_3 again along the latter side. Let us denote by ϑ the dihedral angle formed by the planes on which the two triangles with sides ℓ_1, ℓ_2, and ℓ_4, lie.

The last side, ℓ_3, is a function of such an angle. There are, in particular, two extremal cases corresponding to degenerate tetrahedra, the latterbeing flat, i.e., with zero volume. These two cases correspond to $\vartheta = \pi$ [see Fig. 9(c)], in which case the tetrahedron is completely open and flattened on a plane, and to $\vartheta = 0$ [see Fig. 9(d)], in which case the tetrahedron is completely folded and flattened on a plane.

In the former case $\vartheta = \pi$, we can compute the length of the edge $\overline{bd}$ by considering [see again Fig. 9(c)],

$$\hat{\ell}_3^2 = 4p^2 + 4q^2 = 2\left(\ell_1^2 + \ell_2^2\right) - \ell_4^2, \tag{C7}$$

where we used Eqs. (C6) to relate p and q in function of ℓ_i. Let us observe that the right-hand side of the previous equation is positive because $\ell_1 > \ell_4$.

The remaining case $\vartheta = 0$ can be handled as well to compute the length of the edge $\overline{bd}$ [we use the configuration shown in Fig. 9(d)] and thus get

$$\check{\ell}_3^2 = 4p^2 = \frac{\left(\ell_1^2 - \ell_2^2\right)^2}{\ell_4^2}, \tag{C8}$$

where we again used Eq. (C6) to relate p and q in function of ℓ_i. Let us observe that the right-hand side is trivially positive.

Let us now prove that $\hat{\ell}_3 > \check{\ell}_3$. To achieve this goal, let us consider Fig. 10, where we juxtaposed the two extremal cases. Consider the triangle oTd with a right angle at T, then aO is its hypotenuse, and thus $\overline{Od} > \overline{db}$. But $\hat{\ell}_3 = 2\overline{Od}$ and $\check{\ell}_3 = 2\overline{db}$, hence $\hat{\ell}_3 > \check{\ell}_3$. Let us finally observe that by construction

$$\hat{\ell}_3 < \ell_1 + \ell_2.$$

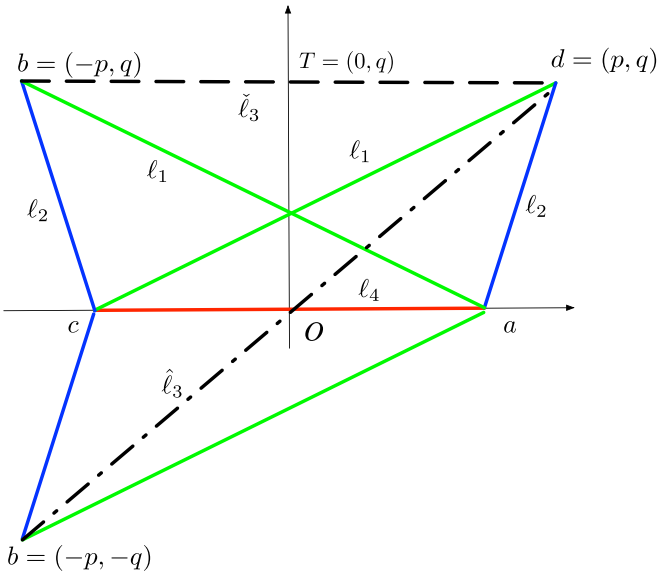

FIG. 10. Two flatten tetrahedra.

We can summarize our findings as follows. Given four sides of length ℓ_i, $i = 1, \ldots, 4$, such that

$$\ell_3 > \ell_1 > \ell_2, \ell_1 > \ell_4, \ell_1 < \ell_2 + \ell_4, \tag{C9}$$

then those sides can be the edges of a tetrahedron if and only if ℓ_3 satisfies

$$\frac{\ell_1^2 - \ell_2^2}{\ell_4} = \check{\ell}_3 < \ell_3 < \hat{\ell}_3 < \sqrt{2\left(\ell_1^2 + \ell_2^2\right) - \ell_4^2}. \tag{C10}$$

Remark 1. Let us conclude by observing that the same result can be obtained by using the Cayley–Menger determinant formula, allowing us to compute the volume of a simplex given its sides. In the present case, the formula returns

$$V^2 = \frac{1}{3!2^3}\begin{vmatrix} 0 & 1 & 1 & 1 & 1 \\ 1 & 0 & \ell_1^2 & \ell_4^2 & \ell_2^2 \\ 1 & \ell_1^2 & 0 & \ell_2^2 & \ell_3^2 \\ 1 & \ell_1^4 & \ell_2^2 & 0 & \ell_3^1 \\ 1 & \ell_1^2 & \ell_3^2 & \ell_3^1 & 0 \end{vmatrix} = \frac{1}{3!2^3}\ell_4^2\left[\ell_3^2 - \frac{\left(\ell_1^2 - \ell_2^2\right)^2}{\ell_4^2}\right]\left[2\left(\ell_1^2 + \ell_2^2\right) - \ell_4^2 - \ell_3^2\right], \tag{C11}$$

where the last equality has been found by using an algebraic manipulator.

[1] F. Battiston, G. Cencetti, I. Iacopini, V. Latora, M. Lucas, A. Patania, J.-G. Young, and G. Petri, Networks beyond pairwise interactions: Structure and dynamics, Phys. Rep. **874**, 1 (2020).

[2] G. Bianconi, *Higher-Order Networks: An Introduction to Simplicial Complexes* (Cambridge University Press, Cambridge, 2021).

[3] C. Bick, E. Gross, H. A. Harrington, and M. T. Schaub, What are higher-order networks? SIAM Rev. **65**, 686 (2023).

[4] V. Salnikov, D. Cassese, and R. Lambiotte, Simplicial complexes and complex systems, Eur. J. Phys. **40**, 014001 (2019).

[5] C. Giusti, R. Ghrist, and D. S. Bassett, Two's company, three (or more) is a simplex: Algebraic-topological tools for understanding higher-order structure in neural data, J. Comput. Neurosci. **41**, 1 (2016).

[6] G. Petri, P. Expert, F. Turkheimer, R. Carhart-Harris, D. Nutt, P. J. Hellyer, and F. Vaccarino, Homological scaffolds of brain functional networks, J. R. Soc. Interface **11**, 20140873 (2014).

[7] A. Patania, G. Petri, and F. Vaccarino, The shape of collaborations, EPJ Data Science **6**, 18 (2017).

[8] A. Patania, F. Vaccarino, and G. Petri, Topological analysis of data, EPJ Data Science **6**, 7 (2017).

[9] S. Majhi, M. Perc, and D. Ghosh, Dynamics on higher-order networks: A review, J. R. Soc. Interface **19**, 20220043 (2022).

[10] G. Bianconi, Quantum entropy couples matter with geometry, arXiv:2404.08556.

[11] Y. Zhou, B. H. Smith, and T. O. Sharpee, Hyperbolic geometry of the olfactory space, Sci. Adv. **4**, eaaq1458 (2018).

[12] C. Giusti, E. Pastalkova, C. Curto, and V. Itskov, Clique topology reveals intrinsic geometric structure in neural correlations, Proc. Natl. Acad. Sci. USA **112**, 13455 (2015).

[13] I. Iacopini, G. Petri, A. Barrat, and V. Latora, Simplicial models of social contagion, Nat. Commun. **10**, 2485 (2019).

[14] G. St-Onge, H. Sun, A. Allard, L. Hébert-Dufresne, and G. Bianconi, Universal nonlinear infection kernel from heterogeneous exposure on higher-order networks, Phys. Rev. Lett. **127**, 158301 (2021).

[15] G. Ferraz de Arruda, M. Tizzani, and Y. Moreno, Phase transitions and stability of dynamical processes on hypergraphs, Commun. Phys. **4**, 24 (2021).

[16] U. Alvarez-Rodriguez, F. Battiston, G. F. de Arruda, Y. Moreno, M. Perc, and V. Latora, Evolutionary dynamics of higher-order interactions in social networks, Nat. Human Behav. **5**, 586 (2021).

[17] T. Carletti, F. Battiston, G. Cencetti, and D. Fanelli, Random walks on hypergraphs, Phys. Rev. E **101**, 022308 (2020).

[18] R. Muolo, L. Gallo, V. Latora, M. Frasca, and T. Carletti, Turing patterns in systems with high-order interaction, Chaos Solitons Fractals **166**, 112912 (2023).

[19] H. Sun and G. Bianconi, Higher-order percolation processes on multiplex hypergraphs, Phys. Rev. E **104**, 034306 (2021).

[20] J. Lee, K.-I. Goh, D.-S. Lee, and B. Kahng, (k, q)-core decomposition of hypergraphs, Chaos Solitons Fractals **173**, 113645 (2023).

[21] M. Mancastroppa, I. Iacopini, G. Petri, and A. Barrat, Hypercores promote localization and efficient seeding in higher-order processes, Nat. Commun. **14**, 6223 (2023).

[22] G. Bianconi and S. N. Dorogovtsev, Theory of percolation on hypergraphs, Phys. Rev. E **109**, 014306 (2024).

[23] G. Bianconi and S. N. Dorogovtsev, Nature of hypergraph k-core percolation problems, Phys. Rev. E **109**, 014307 (2024).

[24] A. P. Millán, H. Sun, J. J. Torres, and G. Bianconi, Triadic percolation induces dynamical topological patterns in higher-order networks, arXiv:2311.14877.
[25] P. S. Skardal and A. Arenas, Abrupt desynchronization and extensive multistability in globally coupled oscillator simplexes, Phys. Rev. Lett. **122**, 248301 (2019).
[26] L. V. Gambuzza, F. Di Patti, L. Gallo, S. Lepri, M. Romance, R. Criado, M. Frasca, V. Latora, and S. Boccaletti, Stability of synchronization in simplicial complexes, Nat. Commun. **12**, 1255 (2021).
[27] P. S. Skardal and A. Arenas, Memory selection and information switching in oscillator networks with higher-order interactions, J. Phys.: Complexity **2**, 015003 (2021).
[28] M. Lucas, G. Cencetti, and F. Battiston, Multiorder Laplacian for synchronization in higher-order networks, Phys. Rev. Res. **2**, 033410 (2020).
[29] L. Gallo, R. Muolo, L. V. Gambuzza, V. Latora, M. Frasca, and T. Carletti, Synchronization induced by directed higher-order interactions, Commun. Phys. **5**, 263 (2022).
[30] T. Carletti, D. Fanelli, and S. Nicoletti, Dynamical systems on hypergraphs, J. Phys.: Complexity **1**, 035006 (2020).
[31] R. Mulas, C. Kuehn, and J. Jost, Coupled dynamics on hypergraphs: Master stability of steady states and synchronization, Phys. Rev. E **101**, 062313 (2020).
[32] Y. Tang, D. Shi, and L. Lü, Optimizing higher-order network topology for synchronization of coupled phase oscillators, Commun. Phys. **5**, 96 (2022).
[33] A. D. Kachhvah and S. Jalan, Hebbian plasticity rules abrupt desynchronization in pure simplicial complexes, New J. Phys. **24**, 052002 (2022).
[34] Y. Zhang, V. Latora, and A. E. Motter, Unified treatment of synchronization patterns in generalized networks with higher-order, multilayer, and temporal interactions, Commun. Phys. **4**, 195 (2021).
[35] A. P. Millán, J. J. Torres, and G. Bianconi, Explosive higher-order Kuramoto dynamics on simplicial complexes, Phys. Rev. Lett. **124**, 218301 (2020).
[36] R. Ghorbanchian, J. G. Restrepo, J. J. Torres, and G. Bianconi, Higher-order simplicial synchronization of coupled topological signals, Commun. Phys. **4**, 120 (2021).
[37] T. Carletti, L. Giambagli, and G. Bianconi, Global topological synchronization on simplicial and cell complexes, Phys. Rev. Lett. **130**, 187401 (2023).
[38] L. Giambagli, L. Calmon, R. Muolo, T. Carletti, and G. Bianconi, Diffusion-driven instability of topological signals coupled by the Dirac operator, Phys. Rev. E **106**, 064314 (2022).
[39] L. Calmon, M. T. Schaub, and G. Bianconi, Dirac signal processing of higher-order topological signals, New J. Phys. **25**, 093013 (2023).
[40] M. Nurisso, A. Arnaudon, M. Lucas, R. L. Peach, P. Expert, F. Vaccarino, and G. Petri, A unified framework for simplicial Kuramoto models, Chaos **34**, 053118 (2024).
[41] A. Arnaudon, R. L. Peach, G. Petri, and P. Expert, Connecting Hodge and Sakaguchi-Kuramoto through a mathematical framework for coupled oscillators on simplicial complexes, Commun. Phys. **5**, 211 (2022).
[42] J. J. Torres and G. Bianconi, Simplicial complexes: Higher-order spectral dimension and dynamics, J. Phys.: Complexity **1**, 015002 (2020).
[43] S. Krishnagopal and G. Bianconi, Topology and dynamics of higher-order multiplex networks, Chaos Solitons Fractals **177**, 114296 (2023).
[44] X. Gong, D. J. Higham, K. Zygalakis, and G. Bianconi, Higher-order connection Laplacians for directed simplicial complexes, J. Phys.: Complexity **5**, 015022 (2024).
[45] R. Muolo, T. Carletti, and G. Bianconi, The three way Dirac operator and dynamical turing and Dirac induced patterns on nodes and links, Chaos Solitons Fractals **178**, 114312 (2024).
[46] S. Barbarossa and S. Sardellitti, Topological signal processing over simplicial complexes, IEEE Trans. Signal Process. **68**, 2992 (2020).
[47] M. T. Schaub, Y. Zhu, J.-B. Seby, T. M. Roddenberry, and S. Segarra, Signal processing on higher-order networks: Livin'on the edge... and beyond, Signal Process. **187**, 108149 (2021).
[48] L. Calmon, S. Krishnagopal, and G. Bianconi, Local Dirac synchronization on networks, Chaos **33**, 033117 (2023).
[49] C. Ziegler, P. S. Skardal, H. Dutta, and D. Taylor, Balanced Hodge Laplacians optimize consensus dynamics over simplicial complexes, Chaos **32**, 023128 (2022).
[50] E. Katifori, G. J. Szöllősi, and M. O. Magnasco, Damage and fluctuations induce loops in optimal transport networks, Phys. Rev. Lett. **104**, 048704 (2010).
[51] G. Gounaris, M. R. Garcia, and E. Katifori, Distribution efficiency and structure of complex networks, arXiv:2111.04657.
[52] G. Gounaris and E. Katifori, A Braess' paradox analog in physical networks of optimal exploration, arXiv:2303.02146.
[53] J. Faskowitz, R. F. Betzel, and O. Sporns, Edges in brain networks: Contributions to models of structure and function, Network Neurosci. **6**, 1 (2022).
[54] A. Santoro, F. Battiston, G. Petri, and E. Amico, Higher-order organization of multivariate time series, Nat. Phys. **19**, 221 (2023).
[55] M. T. Schaub, A. R. Benson, P. Horn, G. Lippner, and A. Jadbabaie, Random walks on simplicial complexes and the normalized Hodge 1-Laplacian, SIAM Rev. **62**, 353 (2020).
[56] L. DeVille, Consensus on simplicial complexes: Results on stability and synchronization, Chaos **31**, 023137 (2021).
[57] L. Calmon, J. G. Restrepo, J. J. Torres, and G. Bianconi, Dirac synchronization is rhythmic and explosive, Commun. Phys. **5**, 253 (2022).
[58] H. Fujisaka and T. Yamada, Stability theory of synchronized motion in coupled-oscillator systems, Prog. Theor. Phys. **69**, 32 (1983).
[59] L. M. Pecora and T. L. Carroll, Master stability functions for synchronized coupled systems, Phys. Rev. Lett. **80**, 2109 (1998).
[60] R. M. D'Souza, M. di Bernardo, and Y.-Y. Liu, Controlling complex networks with complex nodes, Nat. Rev. Phys. **5**, 250 (2023).
[61] V. H. Louzada, N. A. Araújo, J. Andrade, Jr., and H. J. Herrmann, How to suppress undesired synchronization, Sci. Rep. **2**, 658 (2012).
[62] D. Wilson and J. Moehlis, Optimal chaotic desynchronization for neural populations, SIAM J. Appl. Dyn. Syst. **13**, 276 (2014).
[63] C. H. Totz, S. Olmi, and E. Schöll, Control of synchronization in two-layer power grids, Phys. Rev. E **102**, 022311 (2020).

[64] C. Zhou and J. Kurths, Dynamical weights and enhanced synchronization in adaptive complex networks, Phys. Rev. Lett. **96**, 164102 (2006).

[65] R. Berner, S. Yanchuk, and E. Schöll, What adaptive neuronal networks teach us about power grids, Phys. Rev. E **103**, 042315 (2021).

[66] F. Della Rossa, D. Liuzza, F. LoIudice, and P. De Lellis, Emergence and control of synchronization in networks with directed many-body interactions, Phys. Rev. Lett. **131**, 207401 (2023).

[67] M. Asllani, P. Expert, and T. Carletti, A minimally invasive neurostimulation method for controlling abnormal synchronisation in the neuronal activity, PLoS Comput. Biol. **14**, e1006296 (2018).

[68] B. Eckmann, Harmonic functions and boundary value problems in a complex, Comment. Math. Helv. **17**, 240 (1944).

[69] D. Horak and J. Jost, Spectra of combinatorial Laplace operators on simplicial complexes, Adv. Math. **244**, 303 (2013).

[70] H. Nakao, Complex Ginzburg-Landau equation on networks and its non-uniform dynamics, Eur. Phys. J.: Spec. Top. **223**, 2411 (2014).

[71] Y. Kuramoto and H. Nakao, On the concept of dynamical reduction: The case of coupled oscillators, Philos. Trans. R. Soc. London A **377**, 20190041 (2019).

[72] M. Reitz and G. Bianconi, The higher-order spectrum of simplicial complexes: A renormalization group approach, J. Phys. A: Math. Theor. **53**, 295001 (2020).

[73] N. W. Ashcroft and N. D. Mermin, *Solid State Physics* (Saunders College Publishing, New York, 1976).

[74] A. J. Leggett, Lecture 5: Graphene: Electronic band structure and Dirac fermions, Physics 769. Selected Topics in Condensed Matter Physics (2010).